12-2011

Visualizing the Spatial Localization of Active Matrix Metalloproteinases (MMPs) using MALDI Imaging MS

Sasirekha Muruganantham
University of Arkansas, Fayetteville

VISUALIZING THE SPATIAL LOCALIZATION OF ACTIVE MATRIX METALLOPROTEINASES (MMPs) USING MALDI IMAGING MS

VISUALIZING THE SPATIAL LOCALIZATION OF ACTIVE MATRIX METALLOPROTEINASES (MMPs) USING MALDI IMAGING MS

A thesis submitted in partial fulfillment

of the requirements for the degree of

Master of Science in Chemistry

By

Sasirekha Muruganantham

Bharathiar University

Master of Science in Chemistry, 2004

December 2011

University of Arkansas

ABSTRACT

Biomaterial implantation induces the foreign body response (FBR). Development of longer-term implants relies on the thorough understanding of the FBR. The progression of the FBR is regulated by a number of biomolecules including cytokines, chemokines, and matrix metalloproteinases (MMPs). The nature of the FBR requires the spatial and temporal regulation of these mediators. MMPs are an extremely large and diverse group of enzymes that play key roles in regulating the FBR. Precise spatiotemporal regulation of MMPs defines their proteolytic activities. The aim of this project is to develop a new bioanalytical method to visualize the localization of active MMPs at the implant site in *ex vivo* tissue samples.

The localization of active MMP-2 and MMP-9 surrounding the implanted biomaterial in the *ex vivo* tissue sample was determined using MALDI imaging mass spectrometry. The MALDI imaging scheme employed a synthetic FRET substrate specific for MMP-2 and MMP-9. The intensity of the *m/z* value corresponding to the product of active MMP-2 and MMP-9 digestion in each spectrum was extracted to produce a two-dimensional image showing the localization of active MMP-2 and MMP-9 in the *ex vivo* tissue sample. Fluorescence imaging was used as a complementary technique.

This thesis is approved for recommendation
to the Graduate Council.

Thesis Director:

_____

Dr. Julie A. Stenken

Thesis Committee:

_____

Dr. Narayan C. Rath

_____

Dr. Suresh Kumar Thallapuranam

_____

Dr. Paul D. Adams

THESIS DUPLICATION RELEASE

I hereby authorize the University of Arkansas Libraries to duplicate this thesis when needed for research and/or scholarship.

Agreed _____

Sasirekha Muruganantham

Refused _____

Sasirekha Muruganantham

ACKNOWLEDGEMENTS

I would like to express my warmest thanks to all those who helped me understand and execute the goals of this project. No words can express my gratitude to my research advisor, Dr. Julie Stenken, for her immense support and guidance. I would like to thank her for her valuable insights that provoked my thought process. She has been very considerate throughout my graduate program and has motivated me to be an independent researcher.

I am grateful to my committee members, Dr. Narayan Rath, Dr. T.K. Suresh Kumar, and Dr. Paul Adams, for their valuable suggestions throughout my graduate program. I wish to express my sincere thanks to Dr. Jack Lay for granting permission to use the MS facility and for providing the much-needed advice. I appreciate the open door policy he has for students. My heartfelt thanks go to Dr. Rohana Liyanage for providing training and guidance in the MS facility. I would always remember him as my first and best mentor.

I would like to thank Dr. Wayne Kuenzel for allowing me to use the cryostat, Dr. Paul Adams for training me to use the spectrofluorometer, and Dr. Daniel Fologea for training and assisting me with the use of fluorescence microscope and spectrofluorometer. I'm thankful to Dr. Narayan Rath for all the helpful discussions about MMPs and for allowing me to use the humidity chamber.

My special thanks goes to my past postdoctoral group members Dr. Molly Darragh, and Dr. Erika Von Grote for training me on zymography and cryostat, and on probe implantation procedure. I would like to thank all my current and past group members for their helpful suggestions. My sincere thanks go to my husband Arun for help with statistical results

interpretation. I wouldn’t have come this far without his love and care. I would like to extend my thanks to the graduate school and Dr. Julie Stenken for providing funding to attend the 59th ASMS conference. I would like to acknowledge NIH EB 001441 for funding the research.

DEDICATION

This thesis is dedicated to all the laboratory animals that sacrifice their lives for

SCIENCE

TABLE OF CONTENTS

LIST OF FIGURES

LIST OF TABLES

GLOSSARY

ABBREVIATIONS

AEBSF	4-(2-Aminoethyl) benzenesulfonyl fluoride hydrochloride
APMA	p-aminophenylmercuricacetate
CHCA	α-cyano-4-hydroxycinnamic acid
DNP	2,4-dinitrophenyl
ECM	Extracellular matrix
EDTA	Ethylenediaminetetraacetic acid
FAM	Carboxyfluorescein
FBR	Foreign body response
FRET	Förster resonance energy transfer
GPI	Glycosylphosphatidylinositol
IL-8	Interleukin-8
ITO	Indium tin oxide
MALDI-TOF MS	Matrix-assisted laser desorption ionization-time-of-flight mass spectrometry
MCP-1	Monocyte chemoattractant protein-1
MMPs	Matrix metalloproteinases
MNGCs	Multinucleated giant cells
O.C.T.	Optimum cutting temperature
PES	Polyethersulfone
RECK	Reversion-inducing cysteine-rich protein with kazal motifs
TGF-β	Transforming growth factor-β
TIMPs	Tissue inhibitors of metalloproteinases
TNF-α	Tumor necrosis factor- α

1. RESEARCH SIGNIFICANCE AND BACKGROUND

1.1.1 Biomaterials and the foreign body response

Materials used in constructing medical devices such as biosensors, drug-eluting stents, artificial heart valves, and hip prosthesis with a functional life ranging from temporary use to permanent implantation are defined as biomaterials.[1,2] The primary response of the nonspecific immune system evoked by implanted biomaterials is the foreign body response (FBR) or the foreign body reaction.[3]

The FBR is present at the tissue/material interface throughout the *in vivo* lifetime of a medical device and is characterized by a sequence of events including nonspecific adsorption of blood and tissue fluid proteins to the biomaterial surface, formation of blood-based provisional matrix, adhesion of monocytes/macrophages, fusion of macrophages to form multinucleated giant cells (MNGCs), formation of granulation tissue, and eventually formation of fibrous capsule.[2,4] The fibrous capsule confines the implanted biomaterial and prevents it from interaction with the implant site healthy tissue.[2] In some cases, the events in the FBR can render the biomaterial unfit for long-term use.[1]

Several major efforts to engineer biocompatible devices that can avoid the FBR have been unsuccessful due to lack of knowledge of the complex biological effectors of the FBR.[5] It is therefore important to understand the biological nature of the FBR in order to improve the lifetime of the longer-term implanted biomaterial.[6] The progression of the FBR is regulated by a number of mediators including cytokines, chemokines, and matrix metalloproteinases (MMPs) produced by inflammatory cells in the local environment. The outcome of the FBR requires the

spatial and temporal regulation of these mediators. The intricate relationship between the FBR and the expression of these mediators remains to be explored as it is poorly understood.[3] Information about these mediators would eventually aid in understanding the cascade of processes during the FBR and in developing improved long-term biomaterials.

MMPs are a large and diverse group of enzymes (23 human MMPs) that play key roles in regulating the FBR.[7] Several MMPs including MMPs -1,-2,-3,-7,-8,-9,-10, and -12 are involved in different stages of the wound healing process.[8,9] Differences in spatial, temporal, and inducible expression of MMPs indicate their unique roles.[10] Precise spatiotemporal regulation of MMPs confines their diverse proteolytic activities to the necessary conditions and locations.[11]

Few methods are available to determine the localization of active MMPs in biological samples. However, there is no multiplexed assay to visualize the localization of several active MMPs. The aim of this project is to develop a new bioanalytical method to visualize the localization of active MMP-2 and MMP -9 at the implant site in *ex vivo* tissue samples. In the future, this approach can be extended to visualize the localization of several active MMPs at the implant site in *ex vivo* tissue samples.

1.1.2 Role of MMPs in the FBR

During the onset of the FBR, coagulation causes the formation of a blood-based provisional matrix around the implanted biomaterial.[3] In response to the cascade of molecular signals during the inflammatory response, leukocytes migrate through this extracellular matrix (ECM) to reach the inflammation site. Remodeling of the ECM is accomplished by the MMP family to facilitate the migration of leukocytes.[3,12]

Proteolytic MMPs play a role in modulating the adhesion and subsequent fusion of macrophages on the biomaterial surface. The macrophages and the foreign body giant cells adhered to the surface of the biomaterial can secrete active MMPs to modulate the FBR and wound healing.[13]

Moreover, MMPs modulate signaling during the FBR. The ECM serves as a reservoir for various growth factors, and signaling molecules including cytokines, and chemokines. ECM remodeling releases these molecules resulting in the activation of phagocytes.[3]

1.1.3 Role of MMPs in inflammation

MMPs expression has been observed to increase in almost every human disease marked by the presence of inflammation.[14] MMPs are modulators of inflammatory responses.[15] MMPs can either enhance or dampen inflammatory response. MMPs can stimulate inflammation by cleaving the precursors of the pro-inflammatory cytokines TNF-α, IL-1β, and TGF-β.[12,16] On the other hand, MMPs may downregulate inflammation by cleaving chemokines such as MCP-1/CCL2 into their receptor antagonizing mediators.[15,17] Chemokines are a family of chemotactic proteins that facilitate leukocyte chemotaxis by creating a gradient that acts as a guidance signal for the migration of leukocytes.[12] MMP mediated cleavage of chemokines might result in enhancement, inactivation, or antagonism of chemokine activities.[9] Additionally, MMPs might also have an indirect effect on other proteinases that bind, retain, or concentrate chemokines in certain locations.[9,16]

1.1.4 MMPs

MMPs (also called as matrixins) are a family of structurally and functionally related zinc-dependent endoproteinases that are collectively responsible for the degradation of extracellular matrix and non-matrix components during cellular migration and tissue remodeling.[11,18-20] MMPs fall under the metzincin superfamily of metalloproteinases characterized by a catalytic zinc atom in the active site followed by a methionine containing Met-turn.[11,21] Gross and Lapiere were the first to report about MMP-1 in an attempt to establish how a tadpole loses its tail during metamorphosis.[22] To date, there are 24 vertebrate MMPs, and 24 human homologues with two duplicated genes encoding MMP-23.[11,23]

MMPs are synthesized in an inactive pro-form (zymogens).[11] Except MMP-23, all MMPs contain a signal peptide at the N-terminal that leads them to the secretory pathway.[11,24] Then, MMPs can be secreted from the cell or anchored to plasma membrane, thereby confining their catalytic activity to membrane proteins and proteins in the secretory pathway or extracellular space.[11,16] Several MMP family members such as MMP-1, MMP-2, MMP-11, and MMP-13 were found as intracellular proteins, with unclear functions.[22-24] A large number of MMPs are classified into four secreted classes namely collagenase, gelatinase, stromelysin, and matrilysin.[13] Seven MMPs are classified into one of the three membrane-bound classes: type I and type II transmembrane bound, and glycosylphosphatidylinositol (GPI) anchored.[13] Seven MMPs are not classified in to any of the above categories. MMPs are known to perform multiple and overlapping functions.[13] Table 1.1 shows the classifications of MMPs.[11,13]

Main Group	Sub - Group	MMPs
Secreted MMPs	Collagenases	MMP-1, MMP-8, MMP-13, and MMP-18
	Gelatinases	MMP-2, and MMP-9
	Stromelysins	MMP-3, and MMP-10
	Matrilysins	MMP-7, and MMP-26
Other secreted MMPs	_____	MMP-11, MMP-12, MMP-19, MMP-20, MMP-21, MMP-27, and MMP-28
Membrane-type MMPs	Type I transmembrane	MMP-14, MMP-15, MMP-16, and MMP-24
	Type II transmembrane	MMP-23A, and MMP-23B
	GPI anchored	MMP-17, and MMP-25

Table 1.1 Classifications of MMPs[11,13]

The structure of MMPs is composed of several conserved functional domains.[25] Figure 1.1 shows the domain structures of all MMPs.[26,27] All MMPs have 3 domains in common: signal peptide for protein secretion, prodomain for functional regulation, and catalytic domain for substrate processing.[12]

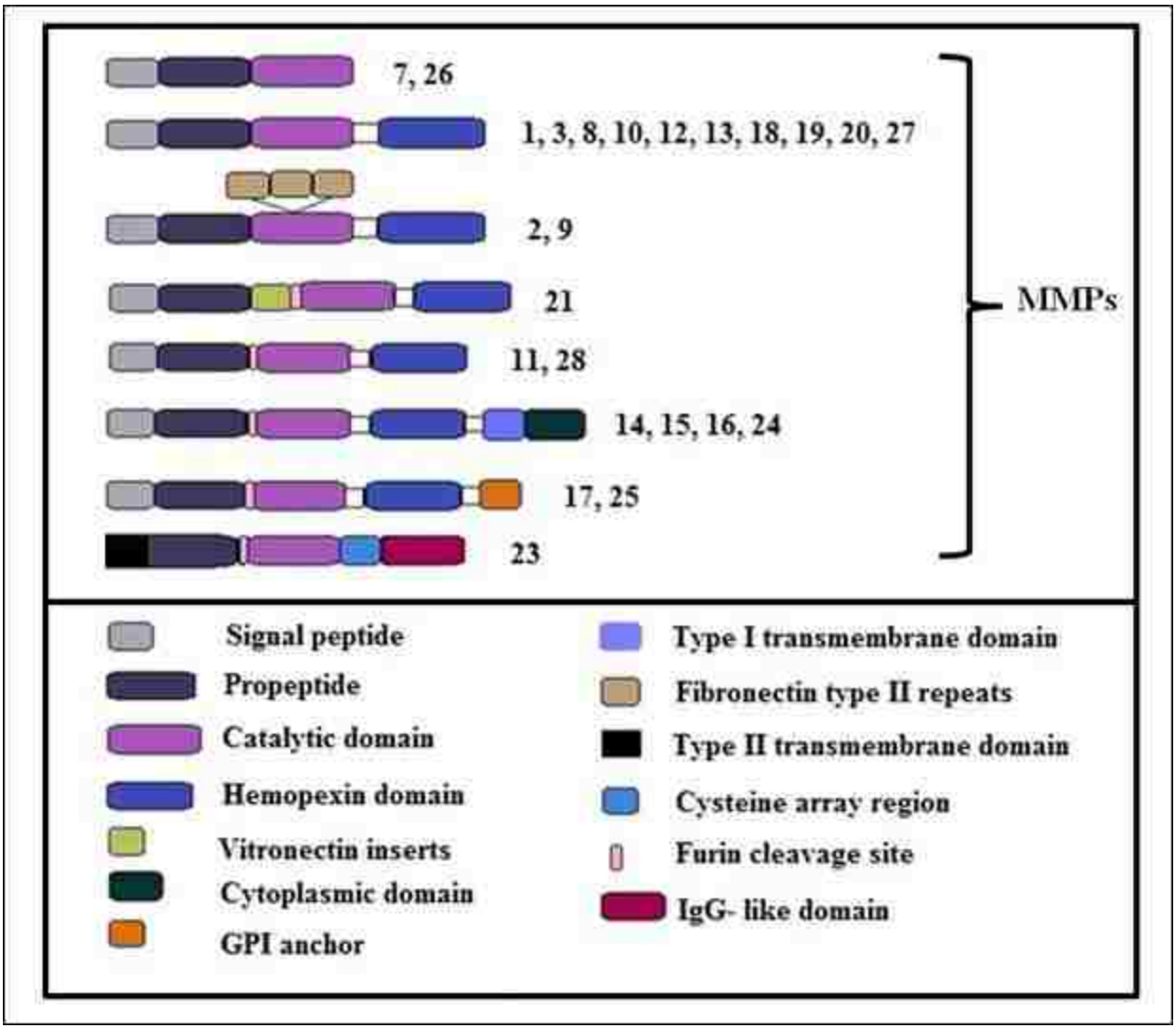

Figure 1.1 Domain structures of 24 vertebrate MMPs (Redrawn from references 26, 27)

The prodomain is ~80 amino acids long and has a conserved sequence PRCXXPD (PHCXXPD in MMP-26), where X may be any amino acid.[28] The cysteine residue within this sequence ligates with Zn^{2+} in the catalytic domain to maintain the proenzyme in a latent form.[25] With the exception of MMP-23, the latency of all MMPs is overcome by disruption of the Cys-Zn^{2+} covalent bond in a "cysteine switch mechanism".[27,29,30] The catalytic domain has ~170

amino acids and a Zn^{2+} binding site HEXXHXXGXXH (where X may be any amino acid), in which the three histidine residues coordinate with the catalytic zinc ion.[31] The catalytic domain also has a structural zinc ion and one or more calcium ions.[32]

With the exception of MMP-7, MMP-23, and MMP-26, all MMPs contain a hemopexin-like domain (~210 amino acids) that is connected to the catalytic domain by a proline-rich hinge region.[16,25,33] The hemopexin domain contributes to substrate recognition, enzyme activation, protease localization, internalization, and degradation.[27,34]

Fibroblasts, endothelial cells, and inflammatory cells including granulocytes, lymphocytes, mast cells, dendritic cells, and monocytes-macrophages are the major source of MMPs.[35] MMPs are synthesized in an inactive pro-form (zymogens) and are activated by other MMP family members or by activators such as serine proteases.[36,37] The activities of MMPs are tightly regulated at different levels namely gene activation and transcription, translation, latent enzyme secretion, proenzyme activation, cell surface localization, and inhibition by endogenous inhibitors like tissue inhibitors of metalloproteinases (TIMPs), reversion- inducing cysteine-rich protein with kazal motifs (RECK), thrombospondin, and α2-macroglobulin.[10,12,25,35,37-40] The effect of posttranslational modification on MMPs activity is not fully understood.[35]

The proteolytic activities of MMPs influence cellular processes including cell proliferation, migration, and adhesion.[11] Maintaining the equilibrium between extracellular matrix deposition and degradation is important for normal tissue development.[19] The fundamental physiological processes that involve tissue remodeling, such as wound healing, angiogenesis, and fetal development depend on the controlled and concerted activity of

MMPs.[11,20] Aberrant regulation of MMPs is implicated in a wide variety of disease states including tumor invasion and metastasis, arthritis, tissue ulceration, periodontitis, and atherosclerosis.[18,20]

1.2 Methods to study the spatial localization of MMPs

1.2.1 Immunohistochemical staining

Two methods are available for performing immunohistochemical staining to identify MMPs in *ex vivo* tissue samples. The direct method is based on the direct application of a primary antibody to the processed tissue whereas the indirect method is based on the identification of an unlabeled primary antibody by a labeled secondary antibody. The latter method is more sensitive and is therefore preferred for the identification of MMPs in local tissue samples. A primary antibody that can specifically recognize the MMP species without cross-reaction with other molecules is desired and therefore monoclonal antibodies are suitable for this purpose. Immunohistochemical staining is limited to a few MMPs because of the non-availability of commercial antibodies specific for all rat MMPs. Nonspecific immunostaining is sometimes obtained in this method. Immunoassays and immunoblotting using tissue homogenates or tissue culture media are some of the other beneficial methods to validate the data and to avoid misinterpretation of false positive and false negative staining.[41] However, these techniques provide quantitative information of total MMPs concentration, but cannot distinguish between pro, active, and TIMP-complexed (inactivated) forms of MMPs.

1.2.2 *In situ* zymography

In situ zymography enables visualization of localized MMPs activities in tissue samples by contacting the tissue section with either a photographic emulsion containing gelatin or a fluorescence-labeled substrate.[42,43] After the incubation period, the activity of MMPs can be seen as white spots in a dark background or as black spots in a fluorescent background.[43] The technique is limited to MMPs-2, -7, and -9.[43]

1.2.3 Fluorescence-based imaging

Förster resonance energy transfer (FRET) MMPs substrates contain two fluorophores situated at a distance of less than 100 Å. The emission wavelength of the donor overlaps with the excitation wavelength of the acceptor and the donor can transfer energy to the acceptor in a non-radiative fashion. Cleavage of the substrate by MMPs relieves the quenching and results in an increase in fluorescence intensity. The change in fluorescence intensity correlates with the activity of MMPs.[44] The technique is limited by the number of fluorophores that can provide non-overlapping emission bands for the products of MMPs activity.

1.2.4 Near Infrared (NIR) fluorescence imaging

Quenched NIR fluorogenic MMPs substrates permit the noninvasive visualization of MMPs activity in whole animals. NIRF substrates were developed based on the FRET mechanism. Cleavage of the substrate by MMPs rescues the quenching and results in an increase in NIR fluorescence intensity.[44,45] Higher penetration of photons emitted by the NIR

fluorophores, and low autofluorescence of the tissues in the NIR spectral region make this technique ideal for tissue imaging.[45]

1.3 Imaging mass spectrometry (IMS)

Immunohistochemistry and fluorescence microscopy are usually employed to image the localization of MMPs within a specific tissue section. Unlike the above-mentioned techniques, IMS uses molecular mass as the endogenous label thereby eliminating the need for special labeling agents.[46] The localized distribution of active MMPs in *ex vivo* tissue samples can be visualized in an indirect manner by monitoring the products formed as a result of activity of MMPs on specific substrates using IMS.

Imaging MS techniques provide information on the identity and spatial distribution of molecules of interest in tissue sections, and single cells.[47,48] Low resolution MALDI-TOF MS images (50–500 μm) indicate the localization of the molecule in a tissue or organ whereas high resolution SIMS-TOF MS images (5–20 μm) provide information about sub-cellular localization of the molecule.[47]

1.3.1 MALDI imaging MS (MALDI-IMS)

Imaging mass spectrometry experiments can be performed on a MALDI-TOF mass spectrometer. Image reconstruction is achieved with custom-made software that also controls the movement of the sample stage over the specified area on the target plate. Sample preparation, sensitivity of the ionization step, spatial resolution, and the speed of the technique (laser repetition rate) influence the analyte localization information obtained using MALDI-IMS.[49]

1.3.2 MALDI-TOF instrumentation

Matrix-assisted laser desorption ionization (MALDI) is a soft ionization technique in which the sample is co-crystallized with a solid matrix that absorbs at the wavelength of the laser. The gas-phase ions produced by irradiating the sample with a pulsed-laser are directed to the mass analyzer.[50]

A time-of-flight (TOF) mass analyzer separates ions based on the differences in their velocities.[50] Ions are accelerated from the ion source into the "field-free" drift region towards the detector. The TOF mass spectrometer measures the time required for an ion to travel from the ion source to the detector. During the instantaneous acceleration process, all the ions receive the same kinetic energy but have different velocities because of the difference in *m/z* values. The ions separate in to groups according to their velocity during their flight through the "field-free" region between the ion source and the detector. In the reflectron mode, an electrostatic mirror is used to reflect ions of the same *m/z* values but with small differences in kinetic energies to improve resolution.[51]

1.3.3 MS/MS spectra using the LIFT technique

MS/MS spectra were obtained using the "LIFT" technique in the MALDI- TOF/TOF mass spectrometer that produces fragment ions by unimolecular decay of the precursor ions without the use of collision gas. Ions coming out of the ion source are subjected to 8 kV accelerating voltage. Fragmentation occurs during the long flight time of the ions. The selected precursor and fragment ions are isolated using a timed ion selector. The ions are then subjected to a potential lift of 19 kV in the "LIFT" device and mass analyzed in a single spectrum.[52]

1.3.4 Working principle

The tissue sample preparation step involves obtaining a thin tissue section of 5-20 µm thickness followed by thaw-mounting the section on to a precooled (-21^0 C) MALDI target plate. Matrix is applied directly to the tissue and allowed to air-dry.[53] A focused pulsed laser beam is rastered across the tissue section.[54] A complete mass spectrum is acquired at specific (x, y) coordinates from the tissue using a TOF mass analyzer. Both the sampling location and the ions detected are recorded. The process is repeated in an ordered array across the tissue surface. The pixels representing the sampling positions are compiled to generate a picture image for each of the detected molecule. Any *m/z* signal is displayed with its relative intensity over the entire array, producing a density map of the molecule in the array area.[53]

1.3.5 Tissue sample preparation

Tissue sample preparation is an important step in tissue analysis by MALDI imaging MS. The objective of the sample preparation step is to get MS-compatible tissue samples.[48] Samples should be handled properly from the time of tissue harvest up to mass spectral analysis. Immediate snap-freezing of the dissected tissue prevents proteolytic degradation. Tissue sections of 10-20 µm thickness is normally used for imaging MS work. Ultra thin tissue sections can be very fragile and susceptible to tearing. Thicker tissue sections require longer drying times and affect the performance of the mass analyzer by their insulating properties.[47] Limiting the thickness of tissue sections and avoiding the use of polymer embedding material during the cryomicrotome cutting of the tissue sections is desired. It is beneficial to deposit the tissue section on to a cold slide followed by rapidly warming the tissue and the slide (thaw mounting).

Sections should be completely thawed when mounted on to an ITO-coated glass slide to avoid freezer burn caused by the residual moisture. Tissue sections should be stored at -80^0 C until analysis. [48,55,56]

In this research, placement of tissues on the sample holder without polymer embedding material was not possible because of the small size of the tissues. Tissues were maintained at the desired orientation on the sample holder by using optimum cutting temperature polymer. Great care was taken to keep the tissue surface polymer-free. In case of accidental contamination of the tissue surface with the polymer embedding material, the 70/30 v/v% ethanol/water wash would dissolve the polymer and keep the tissue surface polymer-free.

1.3.6 Tissue washing step

The objective of the tissue washing step is to wash away contaminants such as optimum cutting temperature (O.C.T.) polymer as well as endogenous molecular species such as lipids and biological salts that might affect the ionization efficiency of the analytes of interest.[48,55] Segregation of salts from the matrix crystals will result in an inhomogeneous sample surface and these local variations can influence the ionization process.[48] The MS signal quality and intensity are improved by the removal of lipids that negatively affect the signal.[57] It is presumed that the solvent washing step will precipitate most proteins *in situ* and localize them within their cellular compartments.[55]

A typical washing step involves the use of ice-cold 70-80% ethanol for the removal of salts. Organic solvents such as chloroform, acetone, hexane, toluene, xylene, and dichloromethane are known to remove lipids.[48] But, there is lack of knowledge of the effect of

these solvents on enzyme activity. The different solvents that were tried in this study (70% ethanol, 80% methanol, and isopropanol) are known to preserve enzyme activity.

1.3.7 Matrix selection and deposition

Selection of an appropriate matrix can enhance the sensitivity of the MS technique towards specific molecules.[48] Matrix deposition should result in homogeneous matrix crystals on the tissue surface without delocalizing the analytes. High resolution tissue imaging requires the formation of matrix crystals on the tissue surface with dimensions smaller than or equal to the diameter of the ionization laser beam. The matrix deposition method should be robust and reproducible.[48,49]

1.3.8 Visualizing the spatial localization of active MMP-2 and MMP-9

The conventional imaging techniques using fluorescence labels cannot be used to monitor the localization of several active MMPs due to the non-availability of longer wavelength fluorophores that provide non-overlapping emission bands for multiplexed MMPs activity. Most of the commercially available shorter wavelength FRET substrates cannot be used for *ex vivo* tissue imaging studies because of the higher autofluorescence of tissues at the wavelengths used. IMS is an emerging technique that eliminates the need for special labeled substrates since it uses molecular mass for identification.

In this research, an indirect MALDI-IMS scheme that employed substrates specific for MMP-2 and MMP-9 was tested to visualize the spatial localization of active MMP-2 and MMP-9 at the implant site in *ex vivo* tissue samples. This novel MALDI-IMS approach for monitoring the localization of active MMP-2 and MMP-9 can be extended to other MMPs by selecting

specific synthetic substrates, thus making this a multiplexed technique to visualize the localization of all active MMPs in *ex vivo* tissue samples. This opens up new possibilities for using IMS as a multiplexed imaging technique for several biological applications.

2. *IN SITU* STUDIES TO IMAGE THE SPATIAL LOCALIZATION OF ACTIVE MMP-9

2.1 Introduction

Enzyme activity, which results in a mass difference between the substrate and its products, can be monitored by mass spectrometry.[58] Initial studies were performed to image the *in situ* enzymatic activity of trypsin on cytochrome c using MALDI-TOF MS.

MMPs have broad and overlapping substrate specificities towards their natural substrates. Synthetic MMPs substrates are advantageous in that they are more specific than the natural MMPs substrates.[59] In this chapter, 2,4-dinitrophenyl(DNP)-Pro-Leu-Gly~Met-Trp-Ser-Arg, a self-quenched FRET peptide substrate specific for the gelatinases MMP-2 and MMP-9, was used for the *in situ* detection of MMP-9 activity using MALDI-TOF MS. The MMP-9 activity assay scheme is shown in Figure 2.1.

GM-6001, a broad spectrum MMPs inhibitor was employed to achieve efficient inhibition of MMP-9 activity *in situ*.[60,61] The inhibition of MMP-9 activity by GM-6001 is crucial to validate the assay scheme for *in vivo* detection of MMPs activity to rule-out proteolytic activities not related to MMPs.

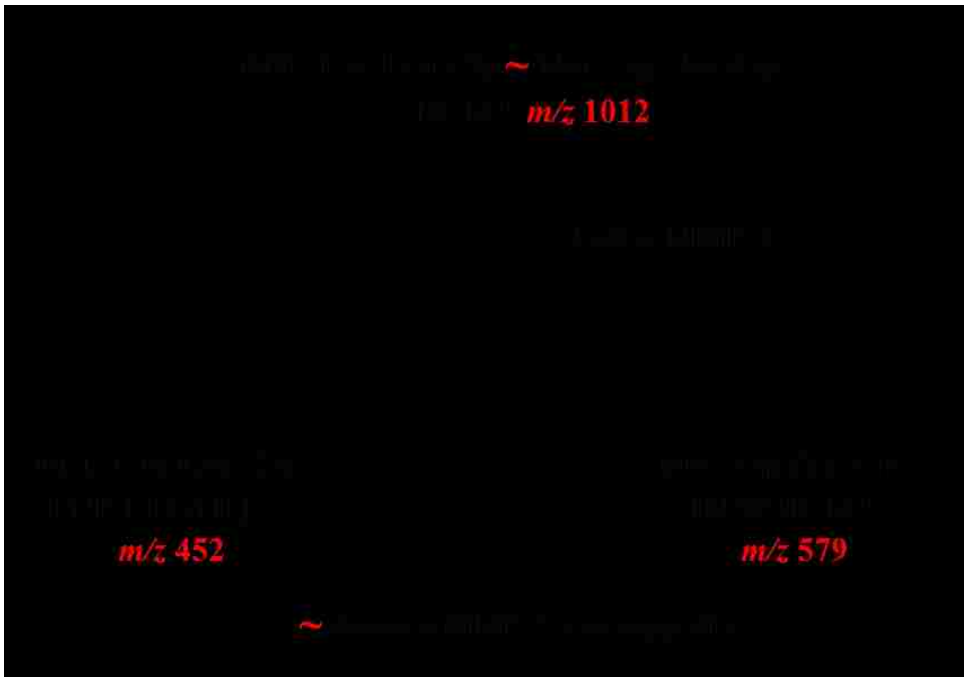

Figure 2.1 MMP-9 activity assay scheme

2.2 Experimental section

2.2.1 Chemicals

Trypsin (Trypsin gold, Mass spectrometry grade) was purchased from Promega (Promega US, Madison, WI, USA). Cytochrome c from bovine heart was purchased from Sigma-Aldrich (St. Louis, MO, USA). MMP-9 (recombinant rat proenzyme, 94 kDa monomer, specific activity > 710 picomoles/min/µg) was purchased from R & D Systems Inc. (Minneapolis, MN, USA). DNP-Pro-Leu-Gly~Met-Trp-Ser-Arg, p-aminophenylmercuricacetate, GM-6001 (Galardin or N-[(2R)-2-(Hydroxamidocarbonylmethyl)-4-methylpentanoyl]-L-tryptophan methylamide, a broad-spectrum MMPs inhibitor), and acetonitrile were purchased from EMD chemicals (Gibbstown, NJ, USA). QXL^{TM}520-Pro-Leu-Gly-Cys(Me)~His-Ala-D-Arg-Lys(5-carboxyfluorescein or

5-FAM)-NH_2, a longer wavelength FRET substrate specific for MMPs-1, -2, -8, - 9, -12, -13 and -14 was purchased from Anaspec (Fremont, CA, USA). Formic acid and HPLC grade water were purchased from Alfa Aesar (Ward Hill, MA, USA). Matrix chemicals, 2,5–dihydroxybenzoic acid (DHB), and α-cyano-4-hydroxycinnamic acid(CHCA) were purchased from Sigma-Aldrich (St. Louis, MO,USA). Indium tin oxide (ITO)-coated glass slides were purchased from Bruker Daltonics Inc. (Billerica, MA, USA). Stock solutions of DNP-Pro-Leu-Gly~Met-Trp-Ser-Arg and QXL^{TM} 520-Pro-Leu-Gly-Cys (Me)~His-Ala-D-Arg-Lys (5-FAM)-NH_2 were prepared in DMSO. Further dilutions were carried out with the assay buffer (50 mM Tris at pH 7.5, 10 mM $CaCl_2$, 1 µM $ZnCl_2$, and 50 mM NaCl).

Novex 10% zymogram (gelatin) gel (1.0 mm, 12 well), LDS sample buffer (4X), MES SDS running buffer (20X), simplyblue safestain (Coomassie G-250 stain), and XCell surelock mini cell system were purchased from Invitrogen (Carlsbad, CA, USA). Prestained protein ladder was purchased from New England Biolabs Inc. (Ipswich, MA, USA). All dilutions were made with HPLC-grade water. Zymography was performed according to the manufacturer's instructions.

2.2.2 (A) MALDI-TOF MS system

Mass spectrometric analyses were performed in the reflectron, positive mode at 25 kV accelerating potential on a Reflex III MALDI-TOF mass spectrometer equipped with a pulsed nitrogen laser working at 337 nm at a laser repetition rate of 8.1 Hz (Bruker Daltonik, Bremen, Germany). The external calibration of the instrument was performed using a solution of peptide calibration standard II (Bruker Daltonics Inc., Billerica, MA,USA) containing angiotensin II, angiotensin I, bradykinin fragment 1-7, substance P, bombesin, ACTH clip 1-17, ACTH clip

18-39, and somatostatin 28, and DHB matrix solution {$[M+H]^+$: 1046.5, 1296.7, 757.4, 1347.7, 1619.8, 2093.1, 2465.2, 3147.5, and 137.0}. The matrix solution was sprayed using an in house-built nebulizer.[62] MS/MS spectra were obtained using the "LIFT" technique with a Bruker Ultraflex II MALDI-TOF/TOF mass spectrometer (Bruker Daltonik, Bremen, Germany).

The analysis was performed using Bruker Flexanalysis 2.4 software. Mass spectral data sets were acquired using the Fleximaging software (Bruker Daltonik, Bremen, Germany) with a raster width of 600 µm. Each pixel composed of 300 individual laser shots collected in 50-shot increments from four positions within a single spot. Molecular images were visualized using the Fleximaging software.

2.2.2 (B) Matrix selection and deposition

Sinapinic acid (SA), 2,5-dihydroxybenzoic acid (DHB), and α-cyano-4-hydroxycinnamic acid (CHCA) are the conventional matrices for imaging MS.[46] Sinapinic acid was not considered for this research as it is the matrix of choice for protein analysis in tissue sections.[49] The matrices, α-cyano-4-hydroxycinnamic acid and 2,5-dihydroxybenzoic acid, were selected as they are well known for highest sensitivity in peptide analysis and for good signal intensity, respectively.[48] The matrices were dissolved in acetonitrile/HPLC grade water (50/50 v/v%) containing 0.1% formic acid.

High resolution tissue imaging requires homogeneous matrix deposition without inducing lateral migration of analytes.[49] The matrix solution was sprayed over the tissue sections using a home-built nebulizer. The spray distance was optimized to avoid excessive wetting of tissue sections marked by dripping of matrix solution from the tissue sections, resulting in

delocalization of analytes. Multiple spray cycles of 150-200 µL were performed up to 8 times on a single tissue section from a distance of approximately 25 cm measured with a ruler. The total volume of the matrix solution per tissue section was 1.5 mL. Tissue sections on the glass slide were air-dried at room temperature for 5 minutes in between the spraying cycles. The time scale of the matrix spraying and drying process was 30 minutes.

2.2.3 MALDI-TOF imaging MS for monitoring the *in situ* localization of trypsin enzymatic activity on ITO-coated glass slides

The localization of trypsin on ITO-coated glass slides was studied using MALDI-TOF imaging MS. The matrix used was 1M 2,5-dihydroxybenzoic acid in acetonitrile/HPLC grade water (50/50 v/v%) containing 0.1% formic acid. The ITO-coated glass slides were marked with a white BIC wite-out shake-N squeeze correction pen (BIC USA Inc., Shelton, CT, USA). Digital images of the sample areas on the slides were acquired using the scanner of a HP Deskjet F4240 All-in-one printer at a resolution of 600 ppi (Hewlett-Packard Company, Palo Alto, CA, USA). [63]

A uniform layer of cytochrome c (2 mg/mL) was applied to ~1 cm^2 square area on the glass slide. Trypsin solution (0.2 mg/mL) was applied to the triangular region on the 1 cm^2 square area. The glass slide was incubated in a humidity chamber at 37^0C for 30 minutes. Peptide calibration standard II (2 µL) from Bruker Daltonics Inc. (Billerica, MA, USA) was spotted beside the 1 cm^2 square area. The matrix solution was sprayed over the dried sample area using an in house-built nebulizer. Multiple spray cycles of approximately 300 µL were performed on the sample area. The total volume of the matrix solution per sample area was 3.0 mL. The

sample areas on the glass slide were air-dried at room temperature for 5 minutes in between the spraying cycles. The time scale of the matrix spraying and drying process was 30 minutes. Sample areas were analyzed using the MALDI-TOF mass spectrometer. The white-out dots were used to teach the software for selecting the imaging area by providing positional information.[63,64]

2.2.4 (A) Activation of MMP-9

MMP-9 was obtained in its proenzyme form and required activation using p-aminophenyl mercuric acetate (APMA). Recombinant rat MMP-9 is converted from a 94 kDa proenzyme to an 84 kDa active enzyme.[65] Pro MMP-9 (530 pM) was incubated with 2.5 mM APMA in assay buffer (50 mM Tris at pH 7.5, 10 mM $CaCl_2$, 1 µM $ZnCl_2$, and 50 mM NaCl) for 2 hours at 37^0C in a sand bath.

2.2.4 (B) Zymography

The activation state of MMP-9 was tested using zymography. An advantage of zymography is that both pro- and active- forms of MMP-9 can be distinguished on the basis of their molecular weight.[66]

APMA-activated MMP-9 samples (25 nM) were mixed with SDS sample buffer and applied to 10% tris-glycine gels with 0.1% gelatin as the substrate. Electrophoresis was performed according to the manufacturer's instructions (Invitrogen, Carlsbad, CA, USA) using XCell surelock mini-cell system at 100 V constant voltage for 130 minutes. After electrophoresis, gels were soaked for 1 hour in 2.5% Triton X-100 to remove SDS. Gels were incubated in zymogram developing buffer (50 mM Tris-HCl with 200 mM NaCl, 5 mM $CaCl_2$,

and 0.02% Brij-35, pH 7.5) for 12 hours at 37^0 C. After incubation, gels were stained with Coomassie G-250 stain for 1 hour and destained in 40/60 v/v% methanol/water with 10/90 v/v% acetic acid/water. Activities of MMP-9 were detected as clear zones against a blue background. In control experiments, GM-6001 (50 μM) was added to the incubation buffer to confirm that the gelatinolytic activity was because of MMP-9. The gels were scanned in a HP scanjet 8300 professional image scanner (Hewlett-Packard Company, Palo Alto, CA, USA) after rinsing with water.

2.2.5 Spectrofluorometer

Fluorescence, resulting from enzymatic activity of MMP-9 on QXL™ 520-Pro-Leu-Gly-Cys(Me)~His-Ala-D-Arg-Lys(5-FAM)-NH_2, was monitored in a Fluoromax-4 spectrofluorometer (Horiba Jobin Yvon Inc., New Jersey, USA) at an excitation wavelength of 490 nm and an emission wavelength of 520 nm.

2.2.6 Fluorescence studies with QXL™ 520-Pro-Leu-Gly-Cys(Me)~His-Ala-D-Arg-Lys (5-FAM)-NH_2

The fluorescence intensity of 10 μM QXL™ 520-Pro-Leu-Gly-Cys(Me)~His-Ala-D-Arg-Lys(5-FAM)-NH_2 was monitored in a spectrofluorometer at an excitation wavelength of 490 nm and an emission wavelength of 520 nm for 5 minutes.[67] Active MMP-9 (4 nM) was added to 10 μM QXL™ 520-Pro-Leu-Gly-Cys(Me)~His-Ala-D-Arg-Lys(5-FAM)-NH_2 and the increase in fluorescence intensity was monitored for 30 minutes (Figure 2.8).

2.2.7 MALDI-TOF MS studies with QXL™ 520-Pro-Leu-Gly-Cys(Me)~His-Ala-D-Arg-Lys(5-FAM)-NH_2

QXL™ 520-Pro-Leu-Gly-Cys(Me)~His-Ala-D-Arg-Lys(5-FAM)-NH_2, a longer wavelength FRET substrate suitable for fluorescence imaging studies, was tested for compatibility with MS. QXL™ 520-Pro-Leu-Gly-Cys(Me)~His-Ala-D-Arg-Lys-(5-FAM)-NH_2 (10 µM) was incubated with active MMP-9 (4 nM) in assay buffer (50 mM Tris at pH 7.5, 10 mM $CaCl_2$, 1 µM $ZnCl_2$, and 150 mM NaCl) in a sand bath maintained at 37^0C. An aliquot of the reaction mixture was removed at various time intervals [0.5, 1, 2, 6, and 12 hour(s)] and mixed with an equal volume of the matrix. The mixture was spotted on a metal MALDI target plate and analyzed using the Bruker Reflex III MALDI-TOF mass spectrometer. The following matrices were used: 1M 2,5-dihydroxybenzoic acid in acetonitrile/HPLC grade water (50/50 v/v%) containing 0.1% formic acid, and 0.1 M α-cyano-4-hydroxycinnamic acid in acetonitrile/HPLC grade water (50/50 v/v%) containing 0.1% formic acid.

2.2.8 (A) LC-MS for monitoring the *in situ* enzymatic activity of MMP-9 in eppendorf vials

A Hewlett Packard 1100 series HPLC (Palo Alto, CA, USA) with a Bruker Esquire 2000 quadrupole ion trap electrospray ionization mass spectrometer (Billerica, MA, USA) was used in the positive ion mode. A bio wide pore C18 reverse phase column (15 cm × 4.6 mm) (Supelco, St. Louis, MO, USA) was used for the separation of analytes. Solvent A contained 0.1% formic acid in water and solvent B contained 0.1% formic acid in acetonitrile. The mobile phase flow rate was 0.8 mL/min with a 5-100% gradient of 0.1% formic acid in acetonitrile over 60 minutes. Samples were injected using an autoinjector with an injection volume of 10 µL. The

mass spectrometer was operated in positive ion mode with 2.1×10^5 Pa nebulizing pressure (N_2), and 12 mL/min flow of drying gas at a temperature of 300^0 C.

2.2.8 (B) MALDI-TOF MS for monitoring the *in situ* enzymatic activity of MMP-9 in eppendorf vials

DNP-Pro-Leu-Gly~Met-Trp-Ser-Arg (50 µM) was incubated with active MMP-9 (530 pM) in assay buffer (50 mM Tris at pH 7.5, 10 mM $CaCl_2$, 1 µM $ZnCl_2$, and 150 mM NaCl) in a sand bath maintained at 37^0C (Figure 2.1). Negative control was performed with 50 µM GM-6001. An aliquot of the reaction mixture was removed at various time intervals [0.5, 1, 2, 6, 12, and 24 hour(s)] and mixed with the matrix. The mixture was spotted on a metal MALDI target plate and analyzed using the Bruker Reflex III MALDI-TOF mass spectrometer. The following matrices were used: 1M 2,5- dihydroxybenzoic acid in acetonitrile/HPLC grade water (50/50 v/v%) containing 0.1% formic acid, and 0.1 M α-cyano-4-hydroxycinnamic acid in acetonitrile/HPLC grade water (50/50 v/v%) containing 0.1% formic acid.

2.2.9 MALDI-TOF imaging MS for monitoring the *in situ* localization of MMP-9 enzymatic activity on ITO-coated glass slides

The localization of active MMP-9 on ITO-coated glass slides was studied using MALDI-TOF imaging MS. The matrices were: 1M 2,5-dihydroxybenzoic acid in acetonitrile/HPLC grade water (50/50 v/v%) containing 0.1% formic acid, and 0.1 M α-cyano-4-hydroxycinnamic acid in acetonitrile/HPLC grade water (50/50 v/v%) containing 0.1% formic acid. The ITO-coated glass slides were marked with white-out. Digital images of the sample areas on the slides were acquired using the scanner of a HP Deskjet F4240 All-in-one printer at a resolution of 600 ppi

(Hewlett-Packard Company, Palo Alto, CA, USA). The matrix solution was sprayed over the dried sample area using an in house-built nebulizer. The spray distance (marked with a ruler) was optimized to avoid excessive wetting of tissue sections, resulting in delocalization of analytes. Multiple spray cycles of 150-200 µL were performed on a sample area from a distance of 25 cm. The total volume of the matrix solution per sample area was 1.5 mL. The sample areas on the glass slide were air-dried at room temperature for 5 minutes in between the spraying cycles. The time scale of the matrix spraying and drying process was 30 minutes. The white-out dots were used to teach the software for selecting the imaging area by providing positional information.

a. Predigested (substrate + active MMP-9) mixture on ITO-coated glass slide

A uniform layer of 50 µM DNP-Pro-Leu-Gly~Met-Trp-Ser-Arg was applied to ~1 cm^2 square area on the glass slide and dried at 37^0C in an oven for 30 minutes. A predigested mixture of [(50 µM DNP-Pro-Leu-Gly~Met-Trp-Ser-Arg + 530 pM active MMP-9), 37^0 C, 24 hours incubation] was applied at the center of the 1 cm^2 square area and dried at 37^0C in an oven for 30 minutes. Peptide calibration standard II (2 µL) from Bruker Daltonics Inc. (Billerica, MA, USA) was spotted beside the 1 cm^2 square area and allowed to dry at room temperature for 5 minutes. After matrix spraying and drying, sample areas were analyzed using the MALDI-TOF mass spectrometer.

b. Incubation on ITO-coated glass slide with active MMP-9

A uniform layer of 50 µM DNP-Pro-Leu-Gly~Met-Trp-Ser-Arg was applied to ~1 cm^2 square area on the glass slide. Active MMP-9 (530 pM) was applied at the center of the 1 cm^2 square area. The glass slide was incubated in a humidity chamber at 37^0C for 24 hours. Peptide

calibration standard II (2 µL) from Bruker Daltonics was spotted beside the 1 cm^2 square area. The matrix solution was sprayed over the sample area of interest. Sample areas were analyzed using the MALDI-TOF mass spectrometer.

2.3 Results and Discussion

2.3.1 MALDI-TOF imaging MS for monitoring the *in situ* localization of trypsin enzymatic activity on ITO-coated glass slides

Trypsin digested 20 µM cytochrome c at the triangular region on the 1 cm^2 square area. Figure 2.2 (A) shows the undigested cytochrome c around the 1 cm^2 square area. The matrix spraying process resulted in delocalization of analytes in the sample area. The MALDI-TOF mass spectrum of cytochrome c is shown in Figure 2.2 (B). The MALDI-TOF mass spectrum of cytochrome c digestion products by trypsin is shown in Figure 2.2 (C).

The sequence of bovine cytochrome c was obtained from www.expasy.org:

GDVEK GKKIF VQKCA QCHTV EKGGK HKTGP NLHGL FGRKT GQAPG FSYTD ANKNK GITWG EETLM EYLEN PKKYI PGTKM IFAGI KKKGE REDLI AYLKK ATNE

The sequence of bovine cytochrome c was used in SequenceEditor software (Bruker Daltonik, Bremen, Germany) to generate the theoretical molecular masses of trypsin digestion fragments (Table 2.1). All the fragments except CAQCHTVEK (*m/z* 1018.4) were observed in the mass spectrum. The protonated peak at *m/z* 1168.8 (TGPNLHGLFGR) was considered to represent the tryptic digestion fragment for generating the MALDI-TOF MS

image. The results of this experiment indicated the possibility of imaging localized MMPs activity on ITO-coated glass slides using MALDI-TOF imaging MS.

Range	**$[MH]^+$**	**Sequence**
[1-5]	547.3	GDVEK
[9-13]	634.4	IFVQK
[14-22]	1018.4	CAQCHTVEK
[28-38]	1168.6	TGPNLHGLFGR
[40-53]	1456.7	TGQAPGFSYTDANK
[74-79]	678.4	YIPGTK
[80-86]	779.4	MIFAGIK
[92-99]	964.5	EDLIAYLK

Table 2.1 Theoretical molecular masses of bovine cytochrome c digestion by trypsin (*m/z* 500 - *m/z* 1600)

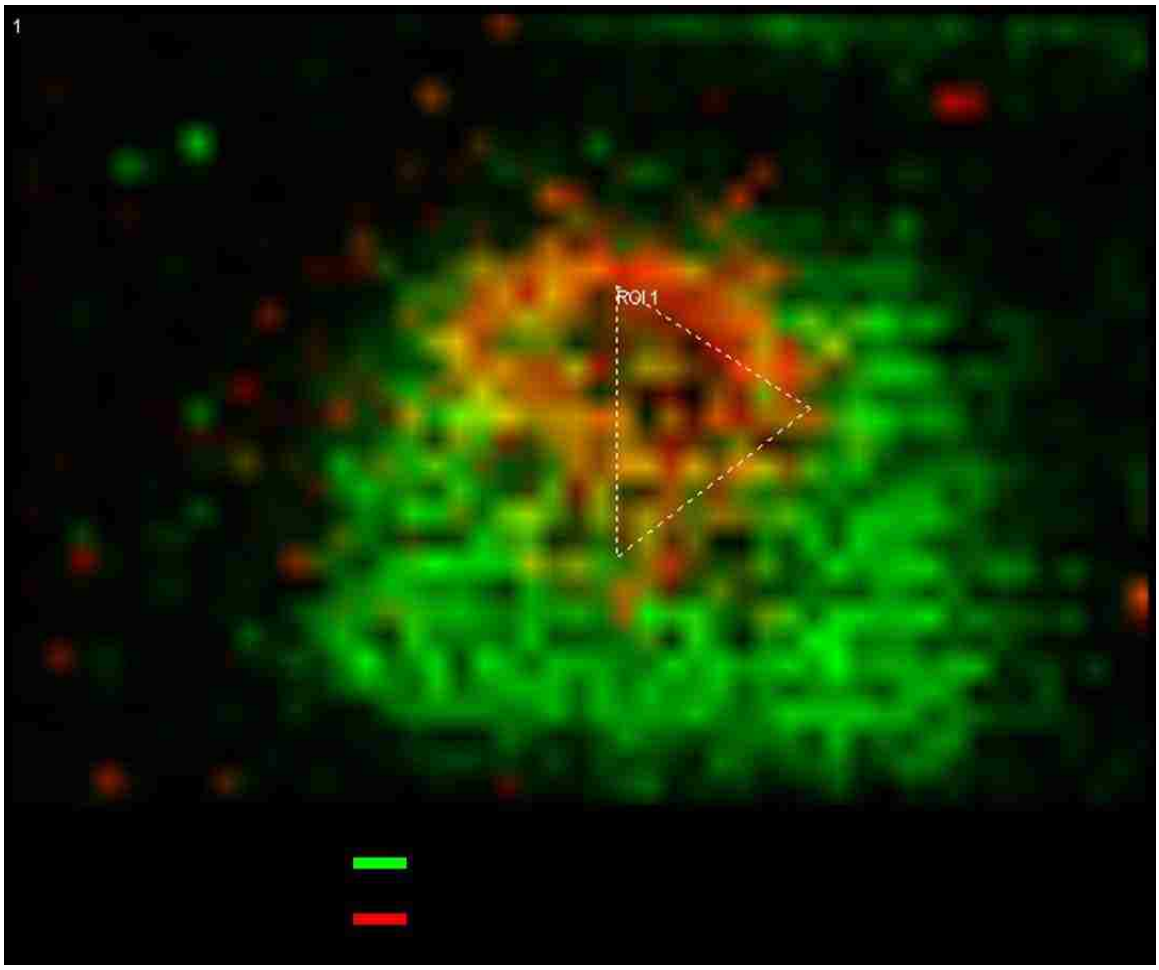

Figure 2.2 (A) MALDI-TOF MS image of i*n situ* digestion on ITO-coated glass slide showing localized trypsin activity at the triangular region (37^0 C, 30 minutes)

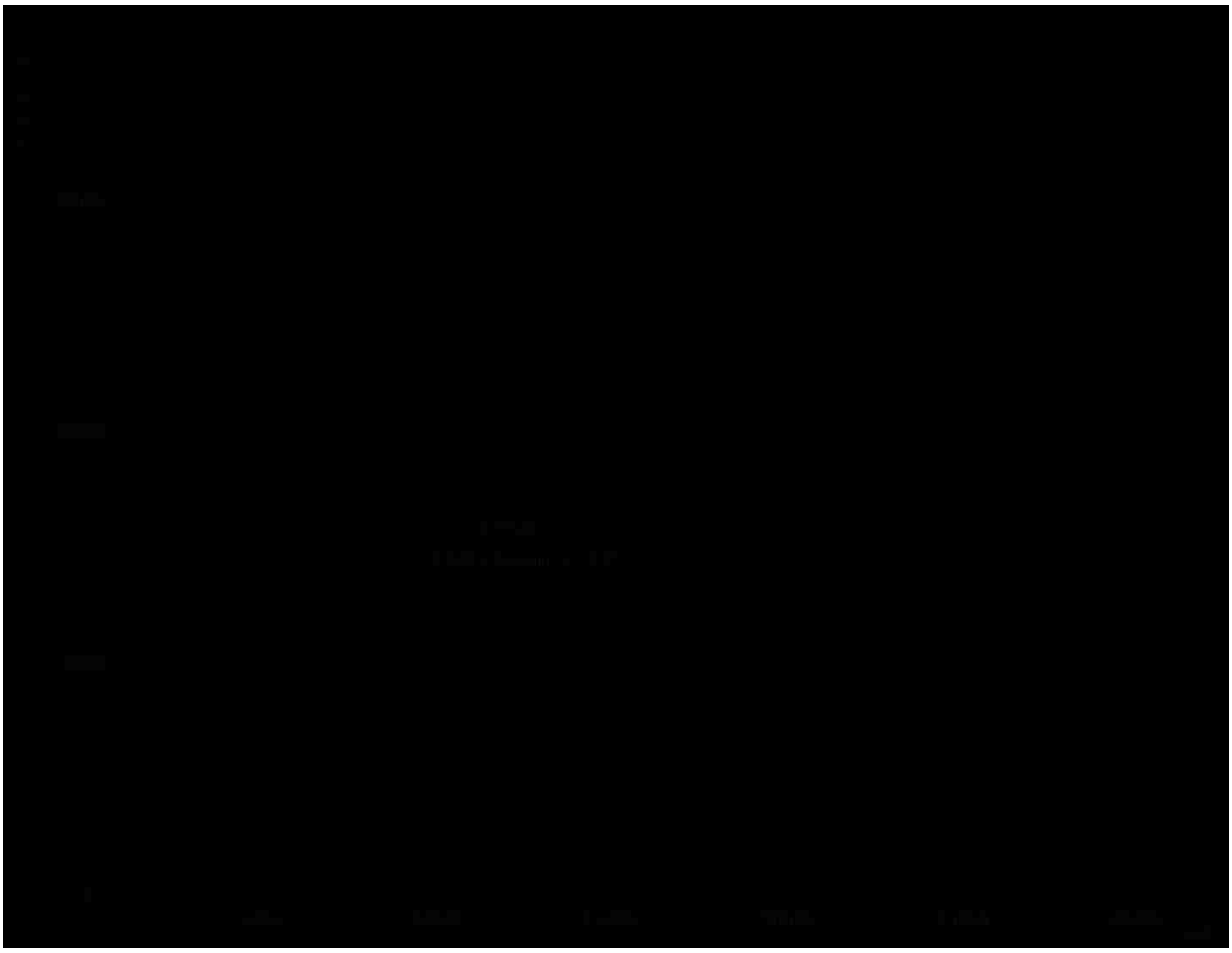

Figure 2.2 (B) MALDI-TOF mass spectrum of cytochrome c (# of laser shots accumulated = 300)

Figure 2.2 (C) MALDI-TOF mass spectrum of cytochrome c digestion products by trypsin (# of laser shots accumulated = 300)

2.3.2 Zymography

Figure 2.3 confirms the activation of 94 kDa pro MMP-9 by APMA in to 84 kDa active MMP-9 visible as clear zones against a blue background.

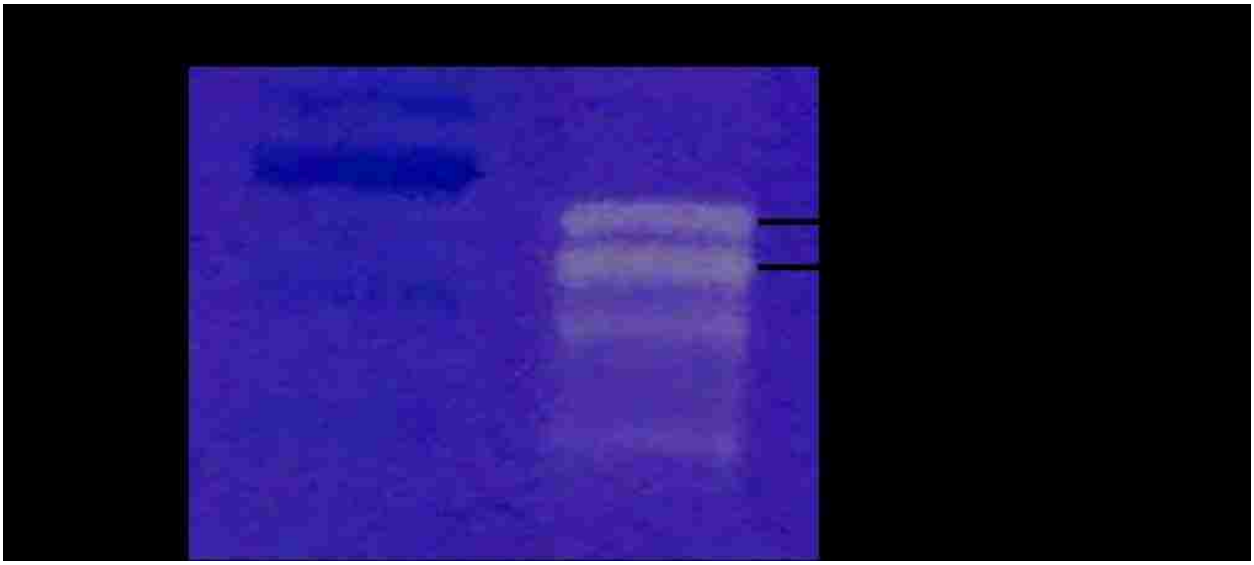

Figure 2.3 Activation of pro MMP-9 by APMA

2.3.3 Fluorescence studies with QXL™ 520-Pro-Leu-Gly-Cys(Me)~His-Ala-D-Arg-Lys (5-FAM)-NH_2

Figure 2.4 shows the fluorescence measurements of enzymatic reaction of active MMP-9 (4 nM) with 10 µM QXL™ 520-Pro-Leu-Gly-Cys(Me)~His-Ala-D-Arg-Lys(5-FAM)-NH_2. The substrate showed negligible background fluorescence signal in the absence of active MMP-9. The results indicated that MMP-9 activity assay could be performed with this FRET substrate.

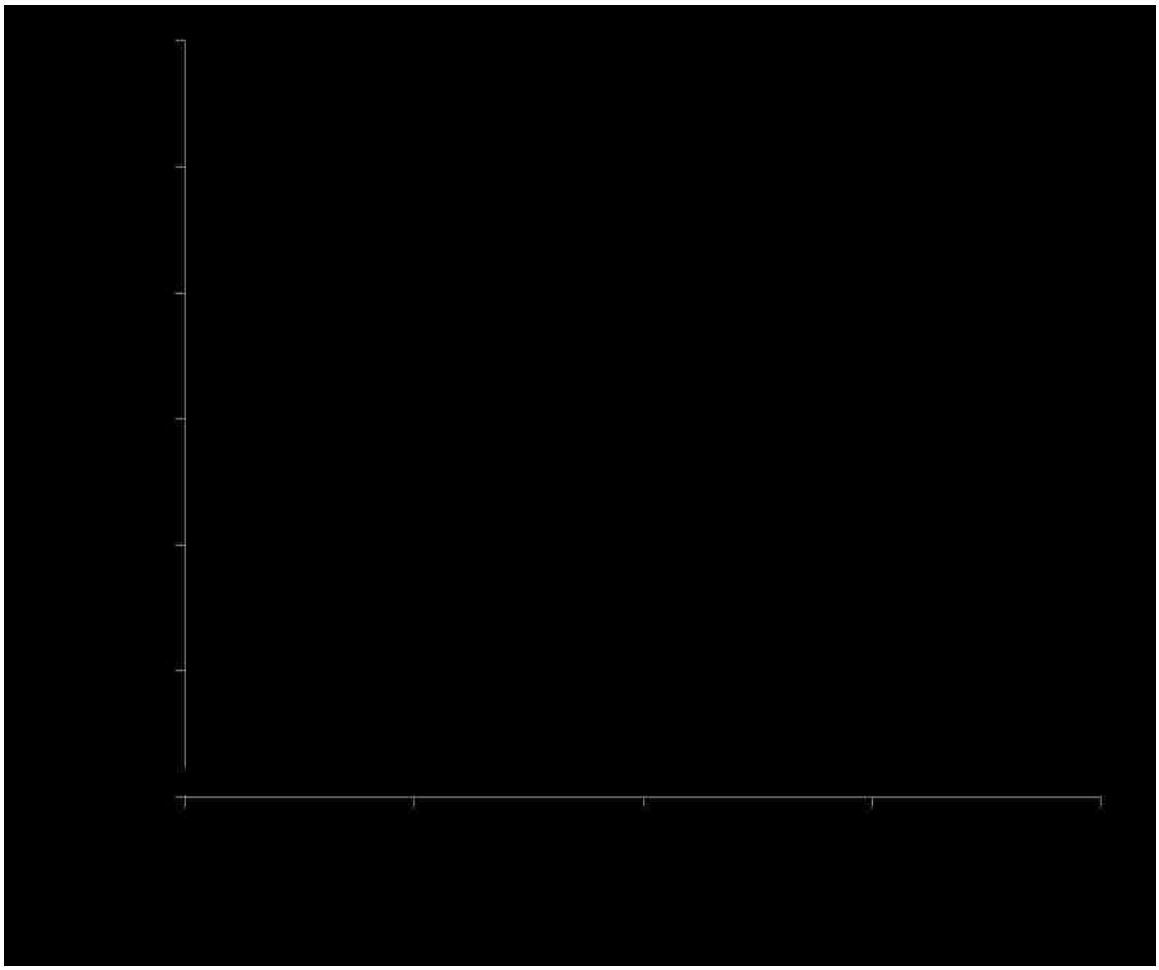

Figure 2.4 Fluorescence measurements of enzymatic reaction of active MMP-9 (4 nM) with 10 µM QXL™ 520-Pro-Leu-Gly-Cys(Me)~His-Ala-D-Arg-Lys(5-FAM)-NH_2 at 37^0 C

2.3.4 MALDI-TOF MS studies with QXL™ 520-Pro-Leu-Gly-Cys(Me)~His-Ala-D-Arg-Lys(5-FAM)-NH_2

Figures 2.5 (A) and 2.5 (B) show the mass spectra of 10 µM QXL™ 520-Pro- Leu-Gly-Cys(Me)~His-Ala-D-Arg-Lys(5-FAM)-NH_2 substrate in DHB (1M 2,5- dihydroxybenzoic acid in acetonitrile/HPLC grade water (50/50 v/v%) containing 0.1% formic acid) and CHCA (0.1 M α-cyano-4-hydroxycinnamic acid in acetonitrile/HPLC grade water (50/50 v/v%) containing 0.1% formic acid) matrix, respectively. The mass spectra did not show intense $[M+H]^+$ peak for the substrate at *m/z* 1744. However, an intense peak at *m/z* 1372 was observed representing the loss of (5-FAM and NH, CH_2 groups of arginine). The QXL™ 520 and 5-FAM modifications at the N- and C-terminus could be responsible for the fragmentation of the substrate.

Figures 2.5 (C) and 2.5 (D) show the mass spectra of [(10 µM QXL™ 520- Pro-Leu-Gly-Cys(Me)~His-Ala-D-Arg-Lys-(5-FAM)-NH_2 + 4 nM active MMP-9), 37^0C, 12 hours incubation] in DHB and CHCA matrix, respectively. The fragmentation products at *m/z* 853 and *m/z* 907 representing the enzymatic activity of MMP-9 on QXL™ 520-Pro-Leu-Gly-Cys(Me)~His-Ala-D-Arg-Lys (5-FAM)-NH_2 were not observed. This could be either because the product ions underwent extensive fragmentation or had lower ionization efficiencies. Hence, this longer wavelength FRET substrate was not used for imaging the activity of MMPs using MALDI-TOF MS.

Figure 2.5 (A) MALDI-TOF mass spectrum of 10 µM QXL^{TM} 520-Pro-Leu-Gly-Cys(Me)~His-Ala-D-Arg-Lys-(5-FAM)-NH_2 in DHB matrix(# of laser shots accumulated = 300)

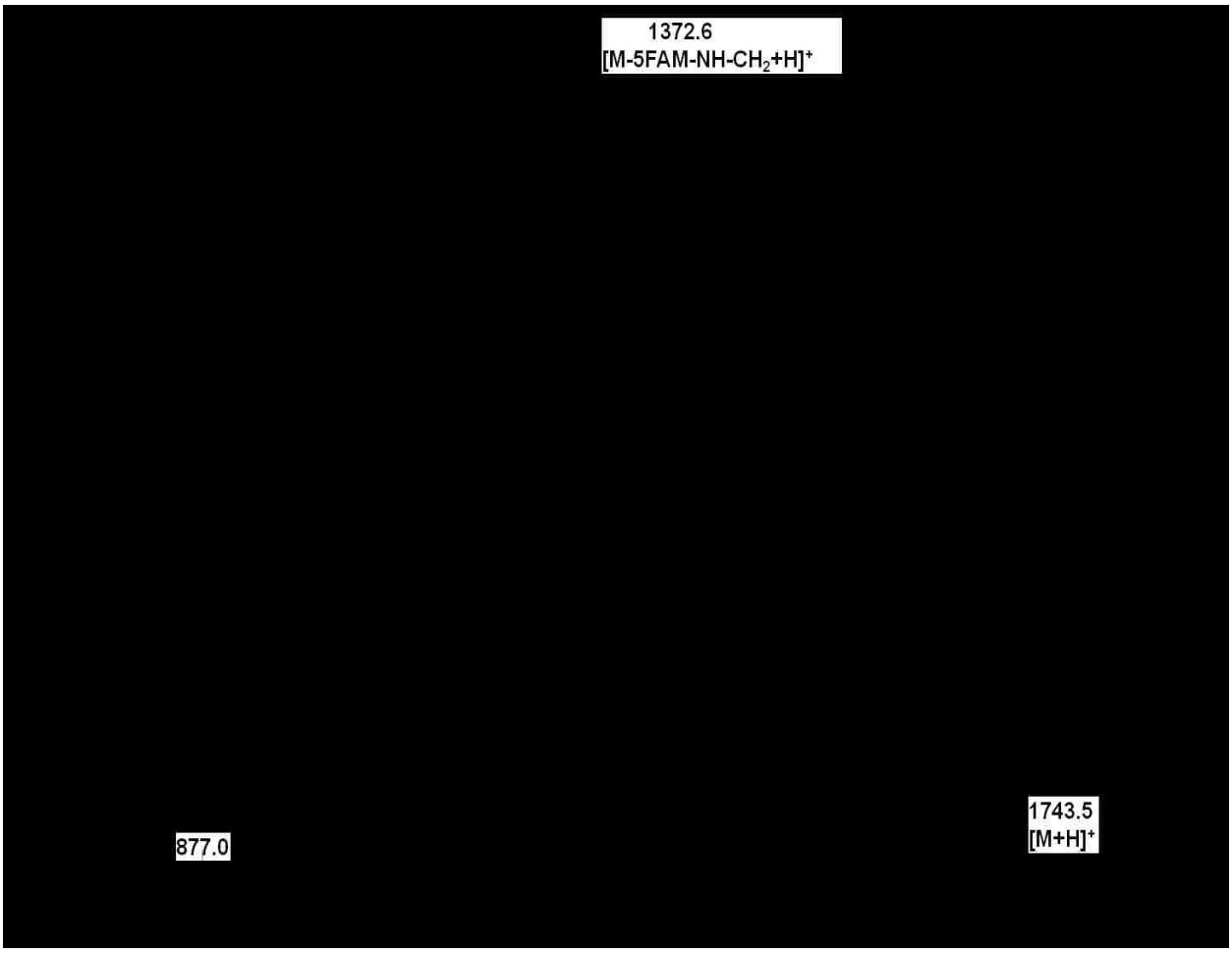

Figure 2.5 (B) MALDI-TOF mass spectrum of 10 µM QXL^{TM} 520-Pro-Leu-Gly-Cys(Me)~His-Ala-D-Arg-Lys-(5-FAM)-NH_2 in CHCA matrix (# of laser shots accumulated = 300)

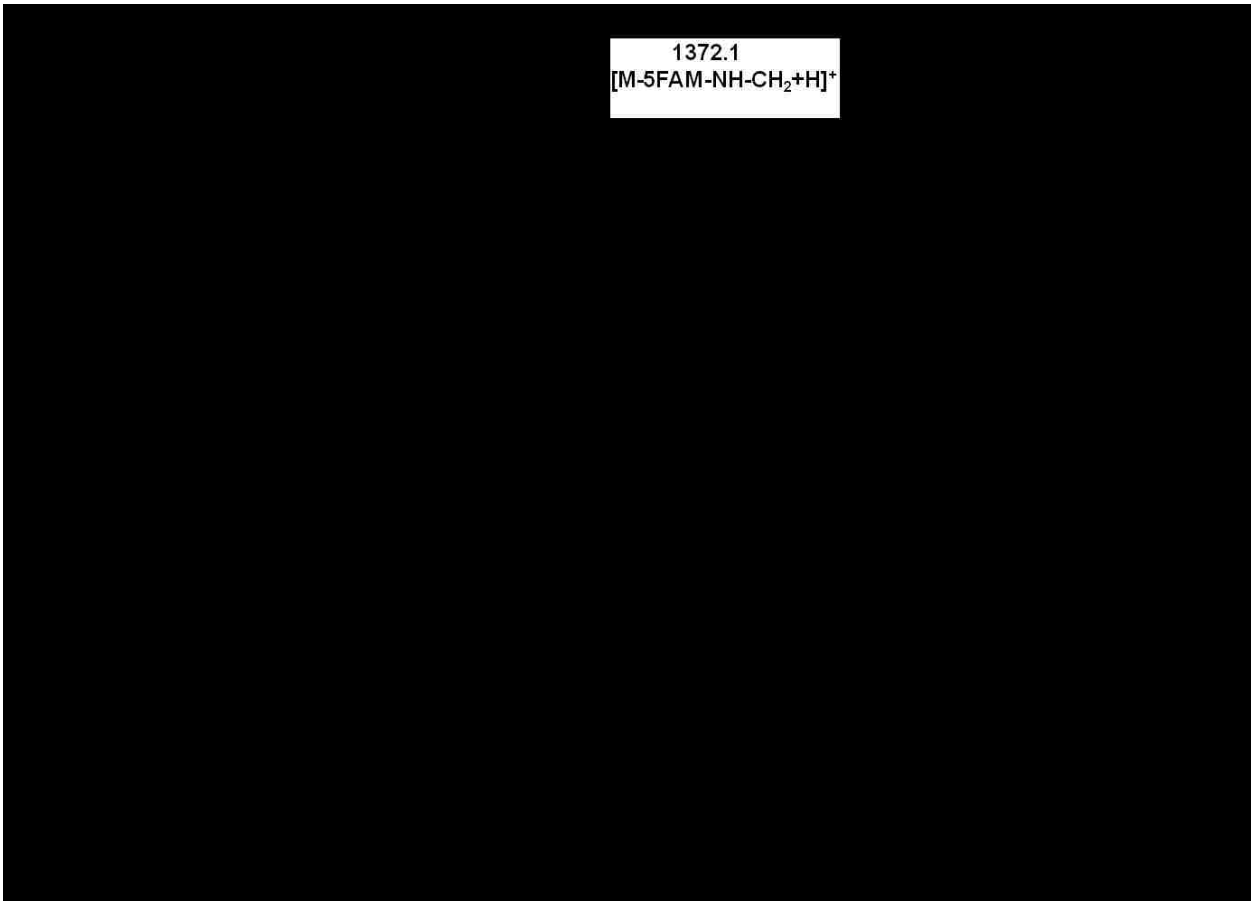

Figure 2.5 (C) MALDI-TOF mass spectrum of [(10 µM QXL^{TM} 520-Pro-Leu-Gly-Cys (Me)~His-Ala-D-Arg-Lys-(5-FAM)-NH_2 + 4 nM active MMP-9), 37^0C, 12 hours incubation] in DHB matrix (# of laser shots accumulated = 1000)

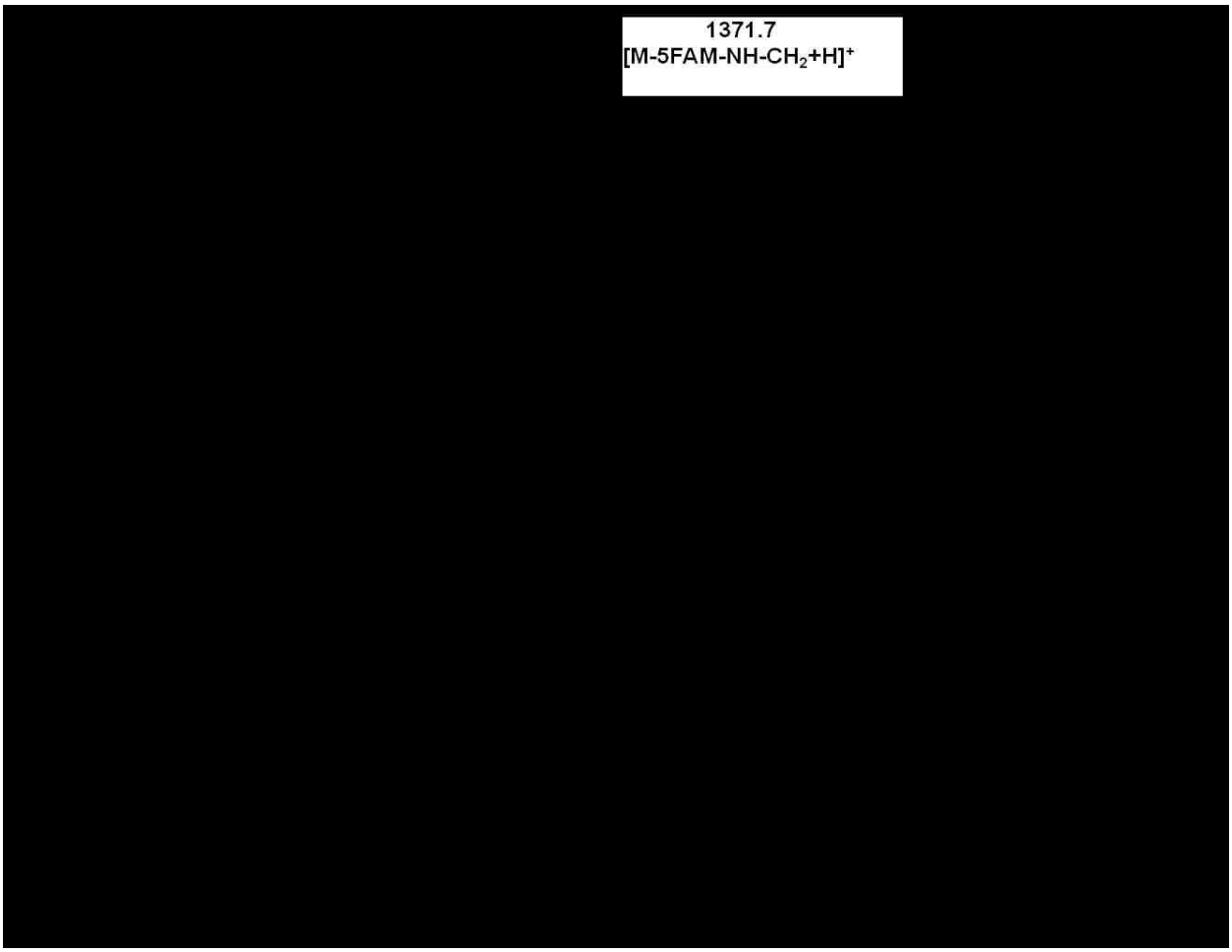

Figure 2.5 (D) MALDI-TOF mass spectrum of [(10 µM QXL^{TM} 520-Pro-Leu-Gly-Cys(Me)~His-Ala-D-Arg-Lys-(5-FAM)-NH_2 + 4 nM active MMP-9), 37^0C, 12 hours incubation] in CHCA matrix (# of laser shots accumulated = 1000)

2.3.5 (A) LC-MS for monitoring the *in situ* enzymatic activity of MMP-9 in eppendorf vials

Figure 2.6 (A) shows the LC chromatogram of the (substrate + active MMP-9) digest (37^0C, 24 hours of incubation) analyzed by LC-ESI-MS. ESI-MS spectra shows [$M+H^+$] peaks for the substrate at *m/z* 1012 [Figure 2.6 (B)], and MMP-9 digestion products at *m/z* 452 [Figure 2.6 (C)] and *m/z* 579 [Figure 2.6 (D)].

Figure 2.6 (A) LC chromatogram of the (substrate + active MMP-9) digest (37^0C, 24 hours of incubation)

Figure 2.6 (B) ESI-MS spectrum of MMP-9 substrate, DNP-Pro-Leu-Gly~Met-Trp-Ser-Arg

Figure 2.6 (C) ESI-MS spectrum of MMP-9 digestion product, DNP-Pro-Leu-Gly

Figure 2.6 (D) ESI-MS spectrum of MMP-9 digestion product, Met-Trp-Ser-Arg

2.3.5 (B) MALDI-TOF MS for monitoring the *in situ* enzymatic activity of MMP-9 in eppendorf vials

QXL^{TM} 520-Pro-Leu-Gly-Cys(Me)~His-Ala-D-Arg-Lys-(5-FAM)-NH_2 was not MS-compatible and therefore MMP-9 activity assay was performed with DNP-Pro-Leu-Gly~Met-Trp-Ser-Arg. Figures 2.7 (A) and 2.7 (B) show the mass spectra of 50 µM DNP-Pro-Leu-Gly~Met-Trp-Ser-Arg substrate in CHCA and DHB matrix, respectively. The DNP modification in the N-terminus of the substrate could have caused the substrate to undergo fragmentation. The mass spectrum of the substrate in CHCA matrix had an intense $[M+H]^+$ peak at *m/z* 1012. The mass spectrum of the substrate in DHB matrix had an intense peak at *m/z* 775 representing the ion formed by the loss of the DNP group and the pyrrolidine ring of proline in the N-terminus of the substrate.

It was possible to monitor one of the hydrolysis products (*m/z* 579) of MMP-9 enzymatic activity on the FRET substrate after 12 hours of incubation at 37^0C [Figures 2.7 (C) and 2.7 (D)]. "LIFT" technique was used to obtain MS/MS data from the *m/z* 579 fragment for confirmation (Figure 2.8). The product peak at *m/z* 579 was not observed in the negative control sample indicating that GM-6001 blocked the activity of MMP-9.

Figure 2.7 (A) MALDI-TOF mass spectrum of 50 µM DNP-Pro-Leu-Gly~Met-Trp-Ser-Arg in CHCA matrix (# of laser shots accumulated = 300)

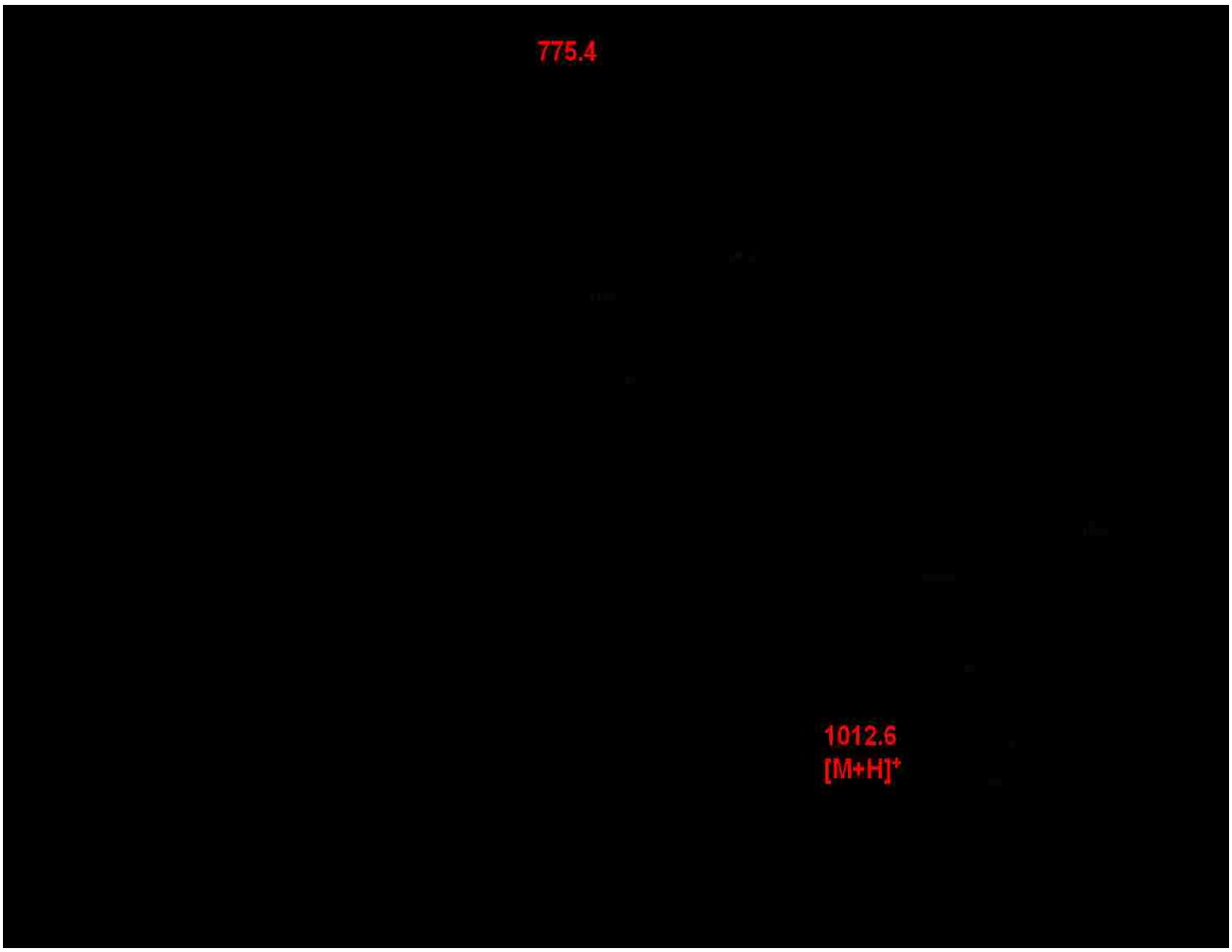

Figure 2.7 (B) MALDI-TOF mass spectrum of 50 µM DNP-Pro-Leu-Gly~Met-Trp-Ser-Arg in DHB matrix (# of laser shots accumulated = 1000)

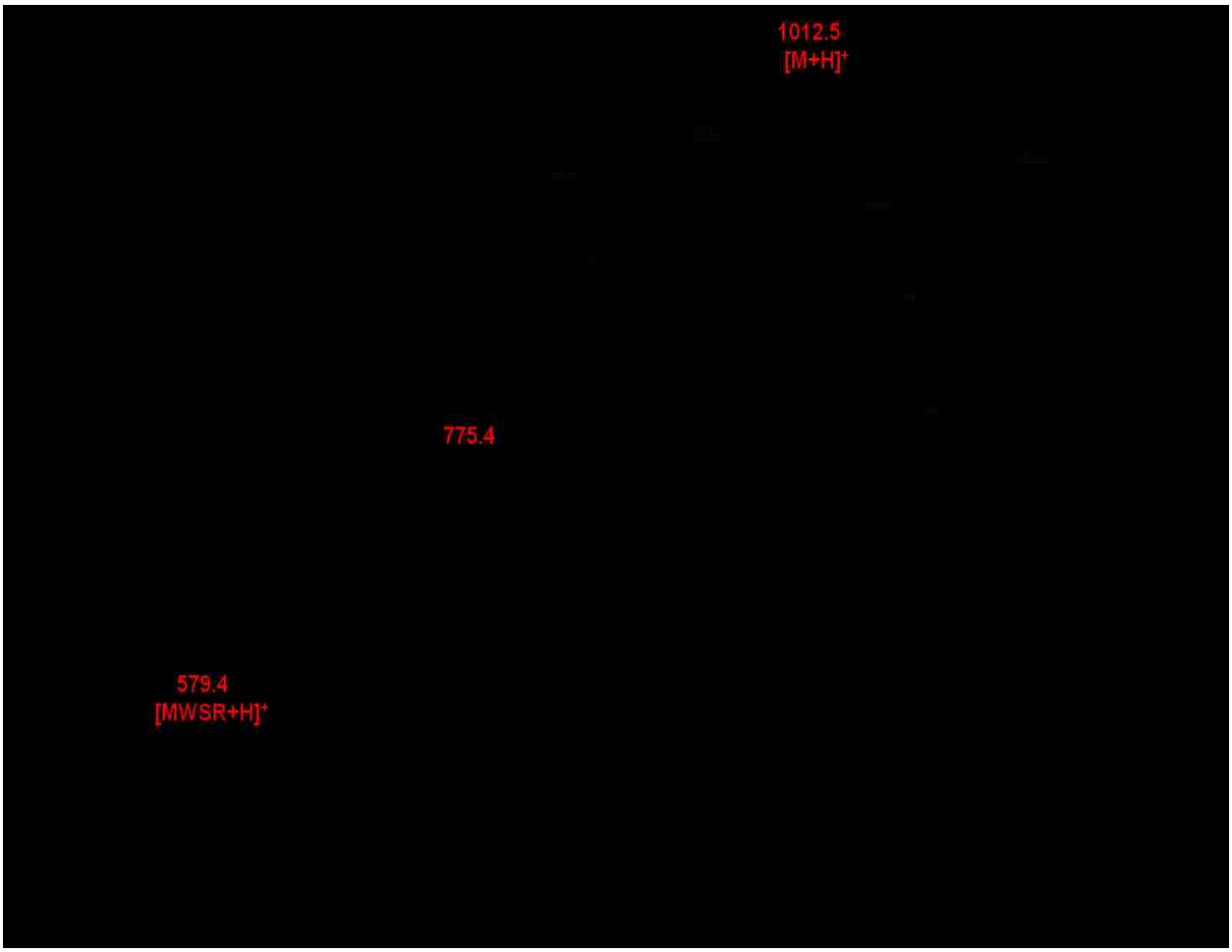

Figure 2.7 (C) MALDI-TOF mass spectrum of product (Met-Trp-Ser-Arg), *m/z* 579 in CHCA matrix (# of laser shots accumulated = 1000)

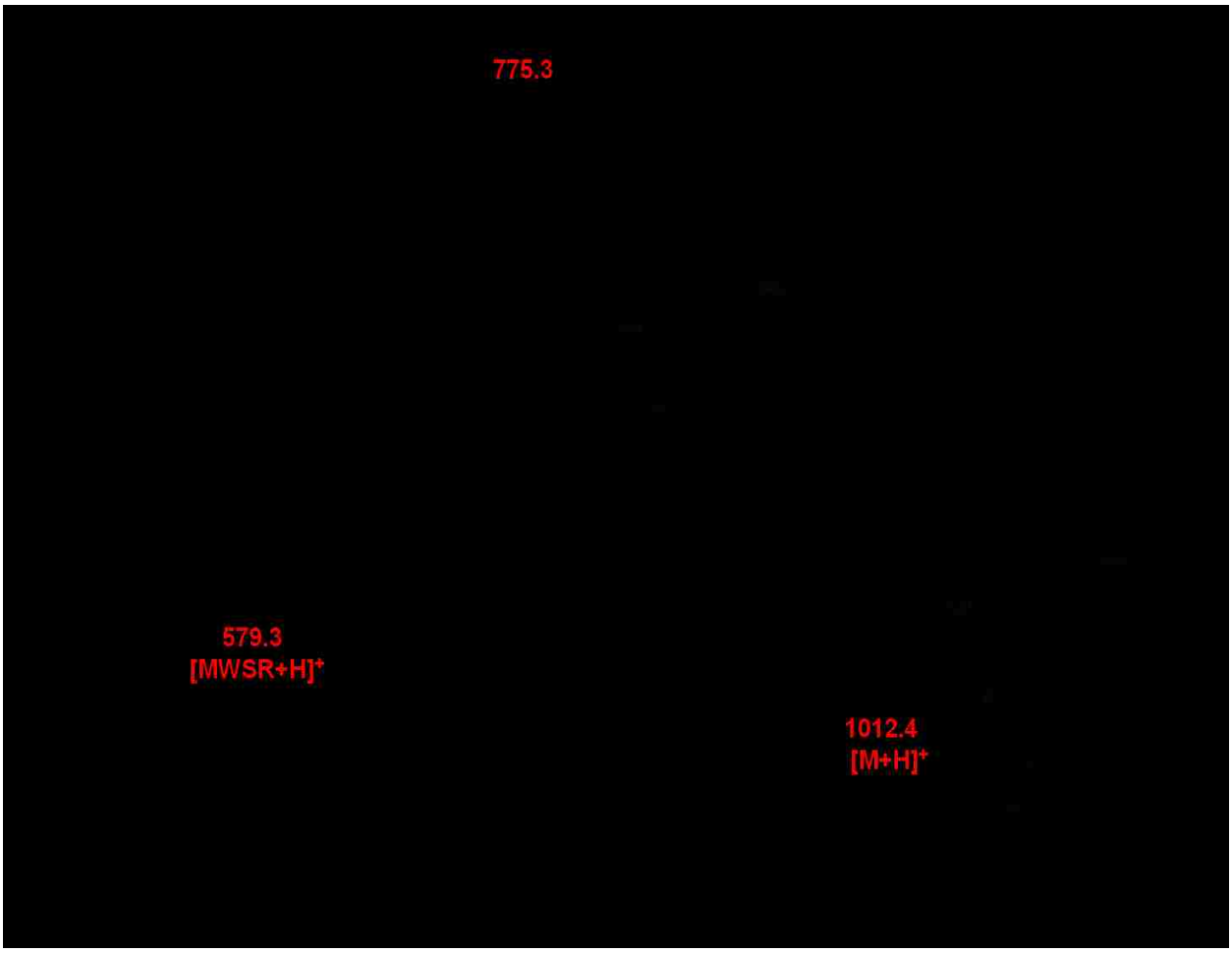

Figure 2.7 (D) MALDI-TOF mass spectrum of product (Met-Trp-Ser-Arg), *m/z* 579 in DHB matrix (# of laser shots accumulated = 1000)

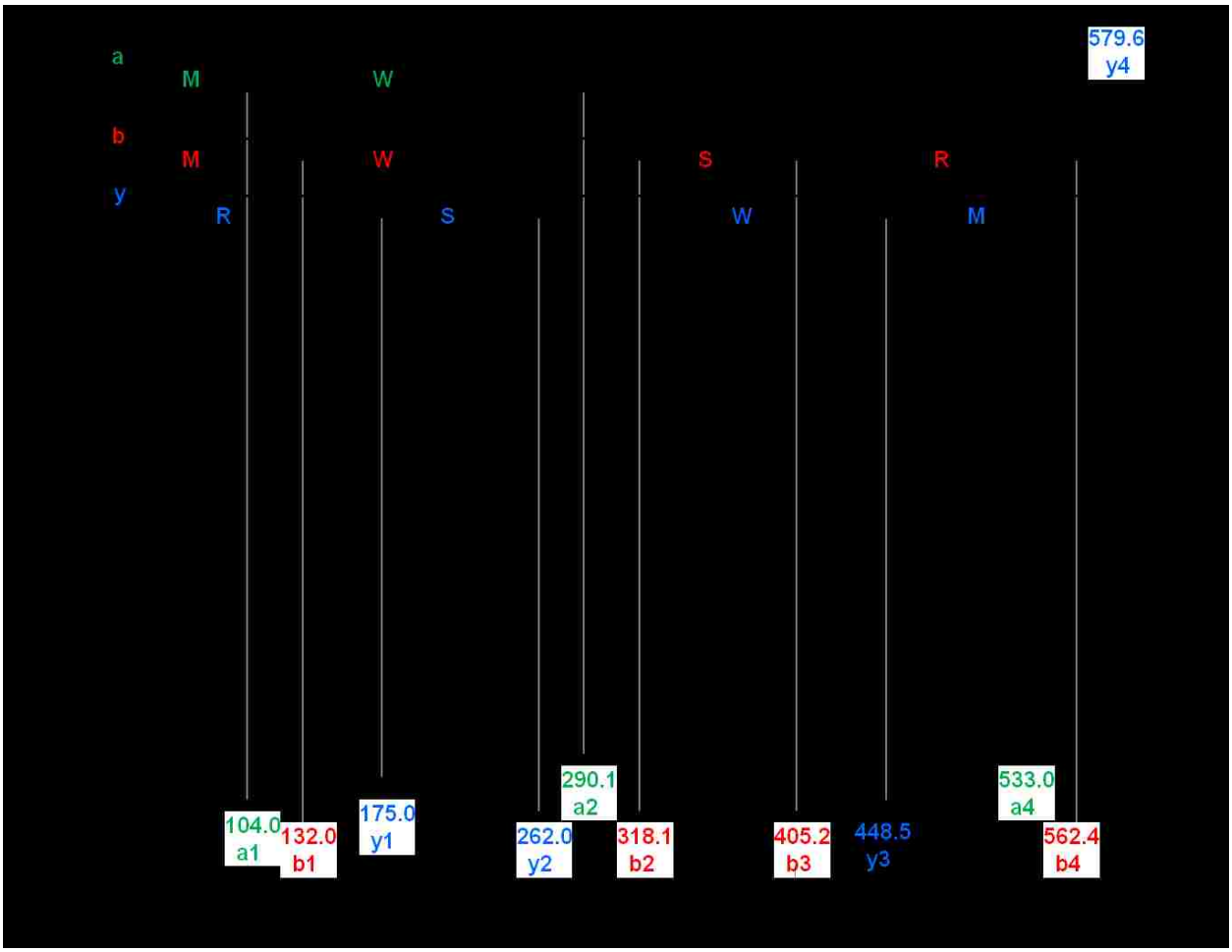

Figure 2.8 MALDI-TOF MS/MS spectrum of the product (*m/z* 579) obtained using the "LIFT" technique

2.3.6 MALDI-TOF imaging MS for monitoring the *in situ* localization of MMP-9 enzymatic activity on ITO-coated glass slides

The substrate fragment at *m/z* 775 (substrate-DNP group-pyrrolidine ring of proline) was considered to represent the undigested substrate in all the *in situ* imaging experiments. It was found that α-cyano-4-hydroxycinnamic acid (0.1 M in acetonitrile/HPLC grade water (50/50 v/v%) containing 0.1% formic acid was not a suitable matrix for the spraying method. The substrate fragment peak at *m/z* 775, and one of the product peaks at *m/z* 579 were not uniformly observed throughout the sample area. The other matrix, 1M 2,5-dihydroxybenzoic acid in acetonitrile/HPLC grade water (50/50 v/v%) containing 0.1% formic acid, produced a homogeneous layer with the sample as evidenced by the uniformity in the distribution of the substrate fragment peak at *m/z* 775, and one of the product peaks at *m/z* 579 throughout the sample area.

a. Predigested (substrate + active MMP-9) mixture on ITO-coated glass slide

When DHB matrix was sprayed from the nebulizer at a distance of 20 cm from the glass slide and with 250-300 µL multiple spray cycles per sample area, the spraying process resulted in delocalization of analytes in the sample area [Figure 2.9 (A)].

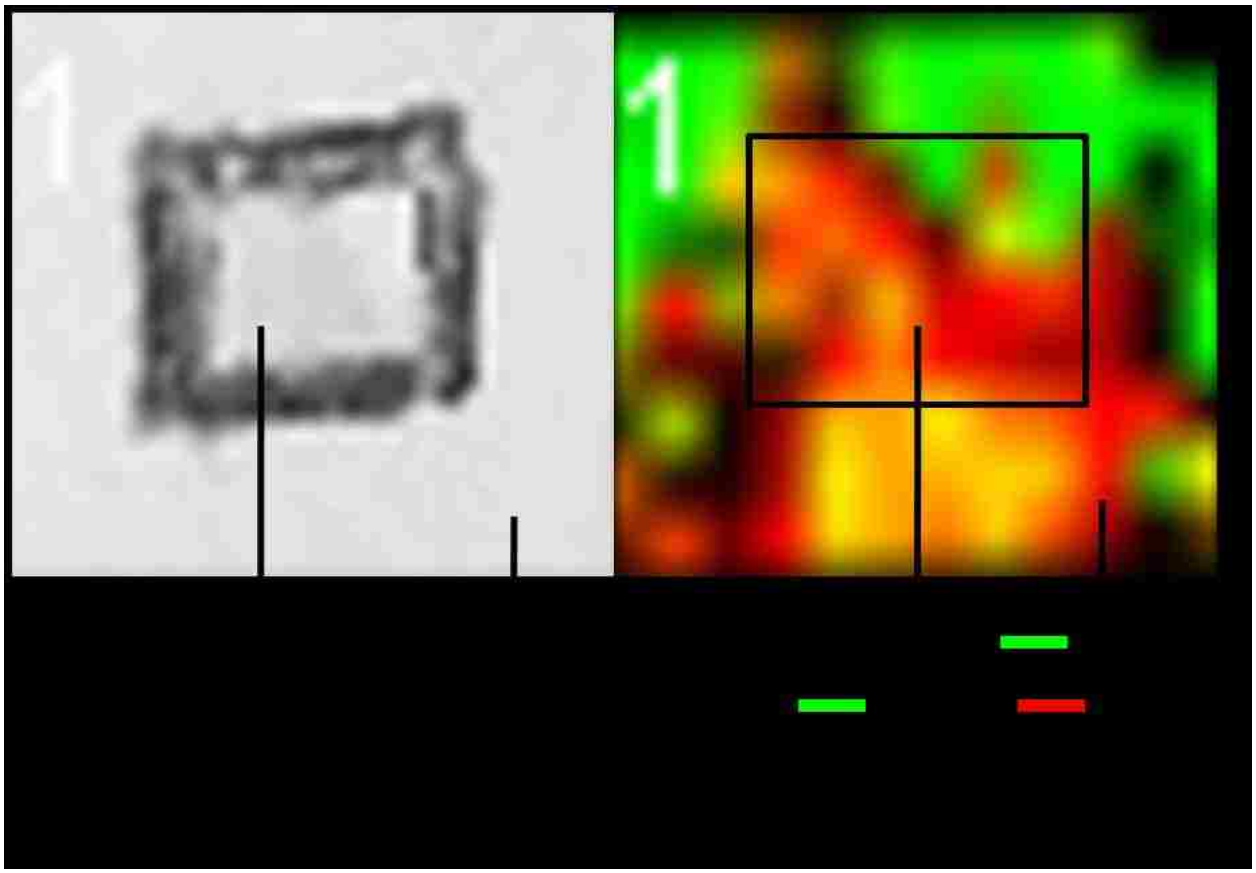

Figure 2.9 (A) MALDI-TOF MS image of predigested (substrate + active MMP-9) mixture on the ITO-coated glass slide (37^0 C, 24 hours of incubation) with a 600 × 600 μm^2 raster

b. Incubation on ITO-coated glass slide with active MMP-9

Active MMP-9 (530 pM) digested 50 µM DNP-Pro-Leu-Gly~Met-Trp-Ser-Arg at the center of the 1 cm^2 square area. Undigested DNP-Pro-Leu-Gly~Met-Trp-Ser-Arg represented by *m/z* 775 is visible around the 1 cm^2 square area [Figure 2.9 (B)].

Optimizing the spraying distance to 25 cm and the volume range of multiple spray cycles to 150–200 µL resulted in homogeneous distribution of the DHB matrix.

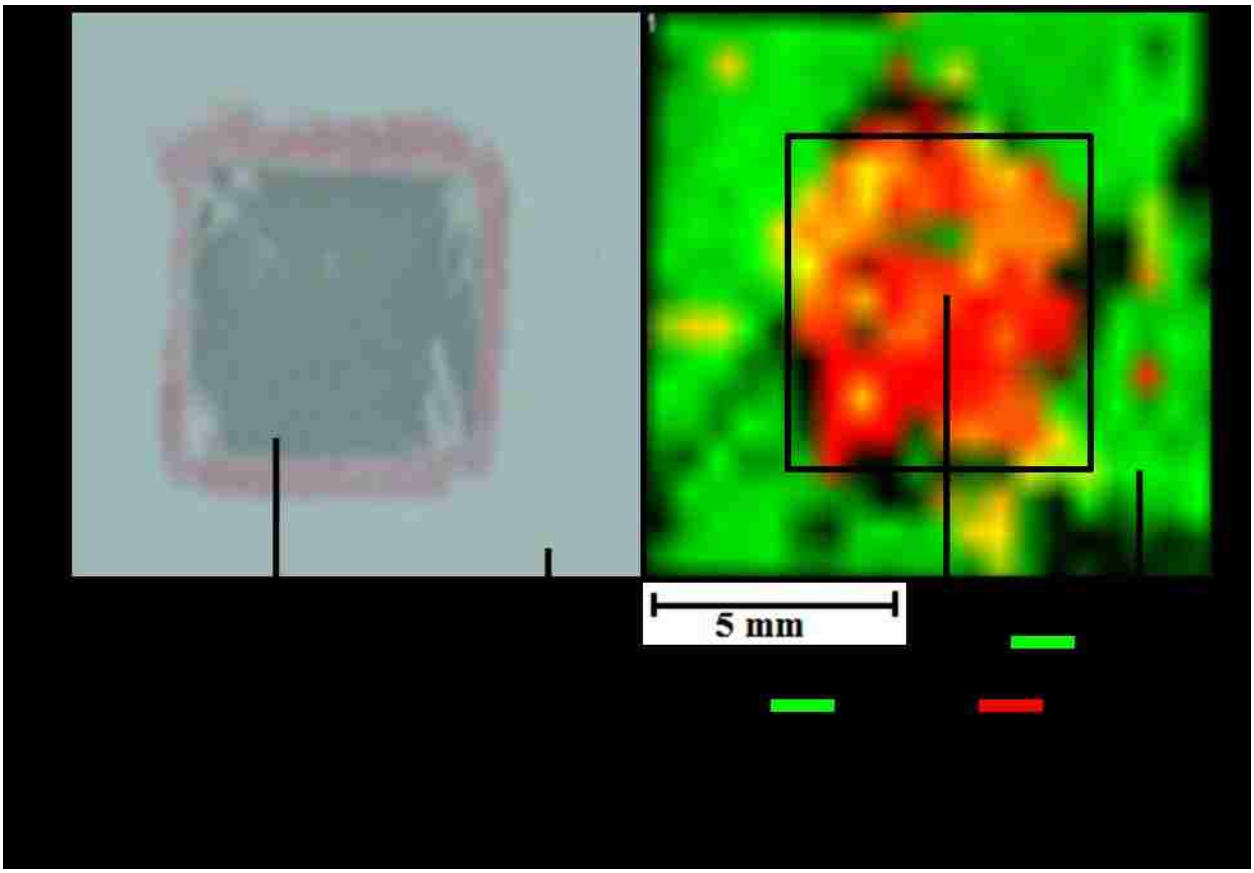

Figure 2.9 (B) MALDI-TOF MS image of i*n situ* digestion on the ITO-coated glass slide with active MMP-9 (37^0 C, 24 hours incubation) with a 600 × 600 μm^2 raster

2.4 Conclusions

LC-ESI MS clearly showed the MMP-9 hydrolysis products at *m/z* 452 and *m/z* 579. However, MALDI-TOF MS did not show the hydrolysis product at *m/z* 452. It was possible to get an image of localized MMP-9 activity on DNP-Pro-Leu-Gly~Met-Trp-Ser-Arg *in situ* by monitoring the hydrolysis product at *m/z* 579 using MALDI imaging MS. The results also indicated that DHB might be a better matrix for *ex vivo* tissue imaging studies. The initial spraying trials resulted in delocalization of analytes in the sample area. In order to avoid this, the spraying distance and the volume required for multiple spray cycles for the matrix solution were optimized for the *in situ* imaging studies. Matrix selection and deposition determined the quality of the MS image. This knowledge was applied when dealing with tissue samples for *ex vivo* imaging studies described in Chapter III.

Higher sensitivity was obtained with a metal MALDI target when compared to the ITO-coated glass slide. However, ITO-coated glass slides are convenient for transferring thin tissue sections from the cryostat during sample preparation for the *ex vivo* tissue imaging studies. Hence, *in situ* imaging studies to monitor localized MMP-9 activity was performed with DNP-Pro-Leu-Gly~Met-Trp-Ser-Arg on ITO-coated glass slides.

3. *EX VIVO* STUDIES TO IMAGE THE SPATIAL LOCALIZATION OF ACTIVE MMP-2 AND MMP-9

3.1 Introduction

In this chapter, DNP-Pro-Leu-Gly~Met-Trp-Ser-Arg was used for the *ex vivo* detection of active MMP-2 and MMP-9 in the FBR-induced tissue samples using MALDI-TOF MS. DNP-Pro-Leu-Gly~Met-Trp-Ser-Arg could not be used for fluorescence imaging because of the high background resulting from the illumination of cells with the UV light. QXL^{TM} 520-Pro-Leu-Gly-Cys(Me)~His-Ala-D-Arg-Lys(5-carboxyfluorescein or 5-FAM)-NH_2, a longer wavelength FRET substrate was used for fluorescence imaging studies.[67] When the peptide is intact, the fluorescence of 5-FAM (donor) is quenched by QXL^{TM} 520 (acceptor) through FRET. Upon cleavage by MMPs in to two separate fragments, the fluorescence of 5-FAM is recovered and can be detected at an excitation wavelength of 490 nm and an emission wavelength of 520 nm.

3.2 Experimental section

3.2.1 Chemicals

MMP-9 (recombinant rat proenzyme, 94 kDa monomer, specific activity > 710 picomoles/min/µg) was purchased from R & D Systems Inc. (Minneapolis, MN, USA). DNP-Pro-Leu-Gly~Met-Trp-Ser-Arg, p-aminophenylmercuricacetate, GM-6001 (Galardin or N-[(2R)-2-(Hydroxamidocarbonylmethyl)-4-methylpentanoyl]-L-tryptophan methylamide, a broad-spectrum MMPs inhibitor), ethanol, methanol, isopropanol, acetonitrile, and DMSO were purchased from EMD chemicals (Gibbstown, NJ, USA). Formic acid and HPLC grade water were purchased from Alfa Aesar (Ward Hill, MA, USA). Matrix chemicals,

2,5–dihydroxybenzoic acid, and α-cyano-4-hydroxycinnamic acid were purchased from Sigma-Aldrich (St. Louis, MO,USA). QXL^{TM} 520-Pro-Leu-Gly-Cys(Me)~His-Ala-D-Arg-Lys (5-carboxyfluorescein or 5-FAM)-NH_2 specific for MMPs-1, -2, -8, - 9, -12, -13 and -14 was purchased from Anaspec (Fremont, CA, USA). Stock solutions of DNP-Pro-Leu-Gly~Met-Trp-Ser-Arg and QXL^{TM} 520-Pro-Leu-Gly-Cys(Me)~His-Ala-D-Arg-Lys(5-FAM)-NH_2 were prepared in dimethyl sulfoxide (DMSO). Further dilutions were carried out with the assay buffer (50 mM Tris at pH 7.5, 10 mM $CaCl_2$, 1 µM $ZnCl_2$, and 50 mM NaCl).

Ethylenediaminetetraacetic acid (EDTA)-free protease inhibitor cocktail (100X) was purchased from Calbiochem (San Diego, CA, USA). 1X solution contains 500 µM 4-(2-Aminoethyl) benzenesulfonyl fluoride hydrochloride (AEBSF), 150 nM aprotinin, 1 µM N-(trans-Epoxysuccinyl)-L-leucine 4-guanidinobutylamide (E-64), protease inhibitor, and 1 µM leupeptin, hemisulfate. This protease inhibitor cocktail inhibits serine and cysteine proteases, but not metalloproteases.[68] The 100X EDTA-free protease inhibitor cocktail was diluted to 1X concentration with HPLC-grade water.

Indium tin oxide (ITO)-coated glass slides were purchased from Bruker Daltonics Inc. (Billerica, MA, USA). Glass coplin staining jars with polypropylene screw cap were purchased from Wheaton science products (Millville, NJ, USA). Tissue-Tek O.C.T. compound was purchased from Sakura Finetek USA, Inc. (Torrance, CA, USA).

3.2.2 Animals

Male Sprague-Dawley rats (260 g to 290 g) were purchased from Harlan laboratories Inc. (Madison, WI, USA) and used in this study.

3.2.3 Biomaterial implantation procedure

Rats were housed in a facility with a 12-hour on/off light cycle and had access to food and water *ad libitum*. All animal experiments were approved by the University of Arkansas animal care committee. Animals were anesthetized with 5% isoflurane (induction) followed by 2% isoflurane (maintenance) inhalation in combination with O_2. Under aseptic conditions, an incision ~1 cm in length was made on each side of the midline along the back of the rat. A subcutaneous pocket was created from each incision by blunt dissection. A microdialysis probe (CMA Microdialysis, North Chelmsford, MA, USA) with a polyethersulfone (PES) membrane was implanted into each pocket. Incisions at the implant site were sealed with Vetbond tissue adhesive (3M Animal Care Products, St. Paul, MN, USA). Following implantation, rats were returned to housing for 24 hours. After 24 hours, the rats were euthanized by CO_2 asphyxiation. Control tissues at a distance of 2 cm from the implants, and the tissues with the implants were cut into 2 cm by 2 cm blocks using sterile scalpel blades.[69]

3.2.4 Tissue sample preparation

After dissection, tissue samples were loosely wrapped in aluminum foil, followed by immediate snap-freezing in liquid nitrogen. Samples were stored at -80^0 C until needed for up to 5 months. The tissue sample was maintained at the desired orientation on the cutting block by using optimum cutting temperature (O.C.T.) polymer. However, the tissue surface was free of the polymer. A thin frozen section of the tissue (20 µm) was cut at -21^0 C using a Leica CM 3050 S cryostat (Leica Microsystems GmbH, Wetzlar, Germany). Sections were thaw-mounted onto precooled (-20^0 C) normal and ITO - coated glass slides and were stored at -80^0 C until analysis. Tissue sections were dehydrated in a vacuum desiccator for 30 minutes. The ITO-

coated glass slides were marked with white BIC wite-out shake-N squeeze correction pen (BIC USA Inc., Shelton, CT, USA). Digital images of the tissue sections on the target plate were acquired using the scanner of a HP Deskjet F4240 All-in-one printer at a resolution of 600 ppi (Hewlett-Packard Company, Palo Alto, CA, USA). The white-out dots were used to teach the software for selecting the imaging area by providing positional information.

3.2.5 MALDI-TOF MS system

Mass spectrometric analyses were performed in the reflectron, positive mode at 25 kV accelerating potential on a Reflex III MALDI-TOF mass spectrometer equipped with a pulsed nitrogen laser working at 337 nm at a laser repetition rate of 8.1 Hz (Bruker Daltonik, Bremen, Germany). External calibration was performed using a solution of peptide calibration standard II (Bruker Daltonics Inc., Billerica, MA, USA) containing angiotensin II, angiotensin I, substance P, bombesin, ACTH clip 1-17, ACTH clip 18-39, and somatostatin 28, and DHB matrix solution {$[M+H]^+$: 1046.5, 1296.7, 757.4, 1347.7, 1619.8, 2093.1, 2465.2, 3147.5, and 137.0}. MS/MS spectra were obtained using the "LIFT" technique in a Bruker Ultraflex II MALDI-TOF/TOF mass spectrometer (Bruker Daltonik, Bremen, Germany).

Spectral acquisition from each spot was achieved using Bruker Flexanalysis 2.4 software. The substrate fragment at *m/z* 775 was considered to represent the undigested substrate. Mass spectral data sets were acquired using the Fleximaging software (Bruker Daltonik, Bremen, Germany) with a raster width of 600 µm. Each pixel composed of 300 individual laser shots collected in 50-shot increments form four positions within a single spot. Molecular images were visualized using the Fleximaging software.

3.2.6 Alcohol-based tissue washing

The solvents used in this study were selected based on their efficacy for lipid solubilization and enzyme activity preservation.[55,70] The following solvents: 70/30 v/v% ethanol/water, 80/20 v/v% methanol/water, and isopropanol were used for tissue washing. Tissue sections were washed by gentle immersing in 70 mL of solvent placed in a glass coplin jar (Wheaton Science Products, Millville, NJ, USA) at 4^0 C for 12 hours. Care was taken to ensure that the coplin jars were undisturbed to prevent diffusion of the endogenous molecules on the tissue surface.[71]

3.2.7 Matrix selection and deposition

The three commonly used matrices for imaging MS studies are sinapinic acid, 2,5-dihydroxybenzoic acid, and α-cyano-4-hydroxycinnamic acid. Sinapinic acid was not considered for this research as it is the matrix of choice for protein analysis in tissue sections. The matrices, α-cyano-4-hydroxycinnamic acid and 2,5-dihydroxybenzoic acid, were selected since they are well known for highest sensitivity in peptide analysis and for good signal intensity respectively.[48] The matrices were dissolved in acetonitrile/HPLC grade water (50/50 v/v%) containing 0.1% formic acid.

High resolution tissue imaging requires homogeneous matrix deposition without inducing lateral migration of analytes.[49] The matrix solution was sprayed over the tissue sections using a home-built nebulizer. The spray distance was optimized to avoid excessive wetting of tissue sections marked by dripping of matrix solution from the tissue sections, resulting in delocalization of analytes. Multiple spray cycles of 150-200 µL were performed on a single

tissue section from a distance of about 25 cm. The total volume of the matrix solution per tissue section was 1.5 mL. Tissue sections on the glass slide were air-dried at room temperature for 5 minutes in between the spraying cycles. The time scale of the matrix spraying and drying process was 30 minutes.

3.2.8 Fluorescence imaging system

Fluorescence imaging studies were performed using an Olympus BH2-RFCA (reflected light fluorescence attachment) microscope.

3.2.9 Imaging active MMP-2 and MMP-9 localization *ex vivo* using FRET substrate

A. MALDI-TOF imaging MS

a. Matrix selection

The product peak at *m/z* 579 was observed in fewer places in α-cyano-4-hydroxycinnamic acid matrix when compared to 2,5-dihydroxybenzoic acid matrix. Hence, DHB was selected as the matrix for all MALDI-TOF imaging MS experiments.

b. Unwashed control tissue

Predigested mixture of [(50 µM DNP-Pro-Leu-Gly~Met-Trp-Ser-Arg + 530 pM active MMP-9), 37^0 C, 24 hours incubation] was applied to the unwashed control tissue on ITO-coated glass slide. Peptide calibration standard II (2 µL) from Bruker Daltonics was spotted beside the tissue section. After acquiring the digital image in a scanner and spraying with DHB matrix, the tissue section was analyzed using the MALDI-TOF mass spectrometer.

c. Ethanol washed control tissue

Ethanol wash is recommended to remove phospholipids, physiological salts, and to fix proteins to increase ion yield in tissue samples.[72] The effect of 70/30 v/v% ethanol/water wash on the activity of MMPs was studied using fluorescence imaging studies. The results from these studies confirmed that the ethanol wash did not affect the activity of MMPs [Figure 3.8 (C)]. Hence, the same solvent system was selected and tested for its effect on MMPs activity and delipidation using MALDI-TOF imaging MS studies.

A specific region of the control tissue on the ITO-coated glass slide was selected and the region was marked underneath the slide using liquid white-out. Active MMP-9 (530 pM) was added to the specific region (red circle). The slide was incubated in an oven at 37^0 C for 15 minutes and was subjected to 70/30 v/v% ethanol/water wash at 4^0C for 12 hours followed by drying at room temperature for 15 minutes. The tissue was covered with assay buffer (50 mM Tris at pH 7.5, 10 mM $CaCl_2$, 1 µM $ZnCl_2$, and 50 mM NaCl) and was allowed to dry in an oven at 37^0 C for 15 minutes. DNP-Pro-Leu-Gly~Met-Trp-Ser-Arg (50 µM) was added to the red circular area and incubated in a humidity chamber at 37^0C for 12 hours (Figure 3.2). After acquiring the digital image in a scanner and spraying with DHB matrix, the tissue section was analyzed using the MALDI-TOF mass spectrometer.

d. Control tissue spiked with predigested (substrate + active MMP-9)

The ITO-coated glass slide with the control tissue was immersed in 70/30 v/v% ethanol/water at 4^0 C for 12 hours followed by drying at room temperature for 15 minutes. The tissue was covered with assay buffer (50 mM Tris at pH 7.5, 10 mM $CaCl_2$, 1 µM $ZnCl_2$, and

50 mM NaCl) and was allowed to dry to dry in an oven at 37^0 C for 15 minutes. The tissue was spiked with predigested [(50 µM DNP-PLG~MWSR + 530 pM active MMP-9), 37^0 C, 24 hours incubation]. After acquiring the digital image in a scanner and spraying with DHB matrix, the tissue section was analyzed using the MALDI-TOF mass spectrometer.

e. Control tissue incubated with (substrate + active MMP-9)

The ITO-coated glass slide with the control tissue was immersed in 70/30 v/v% ethanol/water at 4^0 C for 12 hours followed by drying at room temperature for 15 minutes. The tissue was covered with assay buffer (50 mM Tris at pH 7.5, 10 mM $CaCl_2$, 1 µM $ZnCl_2$, and 50 mM NaCl) and was allowed to dry in an oven at 37^0 C for 15 minutes. The tissue was incubated with [(50 µM DNP-PLG~MWSR + 530 pM active MMP-9)] in a humidity chamber at 37^0 C for 12 hours. After acquiring the digital image in a scanner and spraying with DHB matrix, the tissue section was analyzed using the MALDI-TOF mass spectrometer.

f. Microdialysis probe implanted tissues incubated with substrate

The ITO-coated glass slide with three microdialysis probe implanted tissues was immersed in 70/30 v/v% ethanol/water at 4^0 C for 12 hours followed by drying at room temperature for 15 minutes. Tissues were covered with assay buffer (50 mM Tris at pH 7.5, 10 mM $CaCl_2$, 1 µM $ZnCl_2$, and 50 mM NaCl) and were allowed to dry in an oven at 37^0 C for 15 minutes. The II tissue was incubated with (50 µM DNP-PLG~MWSR+ 1X protease inhibitor cocktail). No treatment (I tissue) and negative control treatment with [(50 µM DNP-PLG~MWSR+ 1X protease inhibitor cocktail + 50 µM GM-6001), III tissue] were also performed. The slide was incubated in a humidity chamber at 37^0 C for 24 hours. After acquiring

digital images in a scanner and spraying with DHB matrix, tissue sections were analyzed using the MALDI-TOF mass spectrometer. "LIFT" technique was used to obtain MS/MS data from the *m/z* 579 fragment for confirmation.

ClinPro Tools software (Version 2.2, Bruker Daltonik GmbH, Bremen, Germany) was used for mass spectral data interpretation. The quick classifier algorithm for automatic peak detection only considered peaks with a signal to noise threshold of 5 with respect to the base peak. Individual peaks in the spectrum from three groups (no treatment, treatment, and negative control treatment) were aligned and peak intensities were analyzed for the *m/z* 579.0 peak.

B. Fluorescence imaging

Fluorescence imaging was initially used to check the effect of alcohol washing on the activity of MMPs. 10 µM QXL^{TM} 520-Pro-Leu-Gly-Cys(Me)~His-Ala-D-Arg-Lys(5-FAM)-NH_2 was applied to the control tissue, and to the probe implanted tissue followed by incubation at 37^0 C in a humidity chamber for 12 hours. Negative control with GM-6001 was included. An EDTA-free protease inhibitor cocktail that prevents the hydrolysis of the substrate by proteinases other than MMPs was employed to validate the activity of MMPs.[73] The tissues were examined under a fluorescence microscope.

3.3 Results & Discussion

A. MALDI-TOF imaging MS

a. Unwashed control tissue

Salts, lipids, and endogenous compounds on the tissue surface can result in "ion suppression" by preferentially capturing protons during the ionization process and appearing at

higher abundance in the spectrum thereby suppressing the signal of other molecules.[74] Phospholipids in the analysis region (*m/z* 575 - *m/z* 579) presented significant challenges in this research by suppressing the product peak at *m/z* 579 indicating the necessity of an appropriate tissue washing procedure to remove interfering lipids (Figure 3.1).

b. Ethanol washed control tissue

MMP-9 activity was localized in the red circular area indicating that the 70/30 v/v% ethanol/water washing did not affect the activity of MMP-9 (Figure 3.2). The interferent phospholipids peaks were less intense and did not suppress the product peak at *m/z* 579 indicating the delipidation efficiency of 70/30 v/v% ethanol/water.

c. Control tissue spiked with predigested (substrate + active MMP-9)

The 70/30 v/v% ethanol/water washed control tissue spiked with predigested MMP-9 product mixture showed the undigested substrate fragment peak at *m/z* 775 and the product peak at *m/z* 579, confirming the delipidation efficiency of 70/30 v/v% ethanol/water (Figure 3.3).

d. Control tissue incubated with (substrate + active MMP-9)

The 70/30 v/v% ethanol/water washed control tissue incubated with (substrate + active MMP-9) mixture showed the undigested substrate fragment peak at *m/z* 775 and the product peak at *m/z* 579, reconfirming the delipidation efficiency of 70/30 v/v% ethanol/water (Figure 3.4).

e. Microdialysis probe implanted tissues incubated with substrate

The substrate fragments at *m/z* 690 and *m/z* 775 were considered to represent the undigested substrate. The 70/30 v/v% ethanol/water washed microdialysis probe implanted tissue without any treatment had background peaks at *m/z* 690 and at *m/z* 775 in certain regions [Figure 3.5 (A) (i)].

The 70/30 v/v% ethanol/water washed microdialysis probe implanted tissue incubated with (50 µM DNP-PLG~MWSR + 1X protease inhibitor cocktail) showed the undigested substrate fragment peaks at *m/z* 690 and *m/z* 775 distributed all over the tissue. The product peak at *m/z* 579 was observed around the microdialysis probe indicating the localization of active MMP-2 and MMP-9 around the microdialysis probe [Figure 3.5 (A) (ii)].

The 70/30 v/v% ethanol/water washed microdialysis probe implanted tissue incubated with (50 µM DNP-PLG~MWSR+ 1X protease inhibitor cocktail + 50 µM GM-6001) showed the undigested substrate fragment peaks at *m/z* 690 and at *m/z* 775 distributed all over the tissue. The product peak at *m/z* 579 was not observed around the microdialysis probe, thus validating the activity assay scheme [Figure 3.5 (A) (iii)].

The MALDI-TOF MS/MS image of 70/30 v/v% ethanol/water washed microdialysis probe implanted tissue incubated with (50 µM DNP-PLG~MWSR + 1X protease inhibitor cocktail) showed the localization of fragments from the unimolecular decomposition of the *m/z* 579 peak around the microdialysis probe [Figure 3.6(A)]. Figure 3.6 (B) shows the MALDI-TOF MS/MS spectrum of the product (*m/z* 579) using the "LIFT" technique.

Using the ClinProTools analysis, P-value from Anderson-Darling test (0.0000357) clearly indicated that the peaks (*m/z* 579) included in the analysis were not normally distributed and thus non-parametric statistical tests are required (Table 3.1). Since the peaks were not normally distributed, the Kruskal-Wallis test was used to determine the significant difference between three group [no treatment, treatment, and negative treatment (GM-6001)] averages. Kruskal-Wallis test resulted in a P-value of 0.0638. The kruskal-wallis test will be highly significant (<0.05) only when all the 3 groups are significantly different from each other. Out of the 3 groups, two groups were not significantly different from each other. Hence, the P-value of 0.0638 that shows a marginal difference among the 3 groups is acceptable. Figure 3.7 (A) and Figure 3.7 (B) compare all single spectra and average spectral intensities of *m/z* 579.0 peak for no treatment (green), treatment (red), and negative treatment (blue).

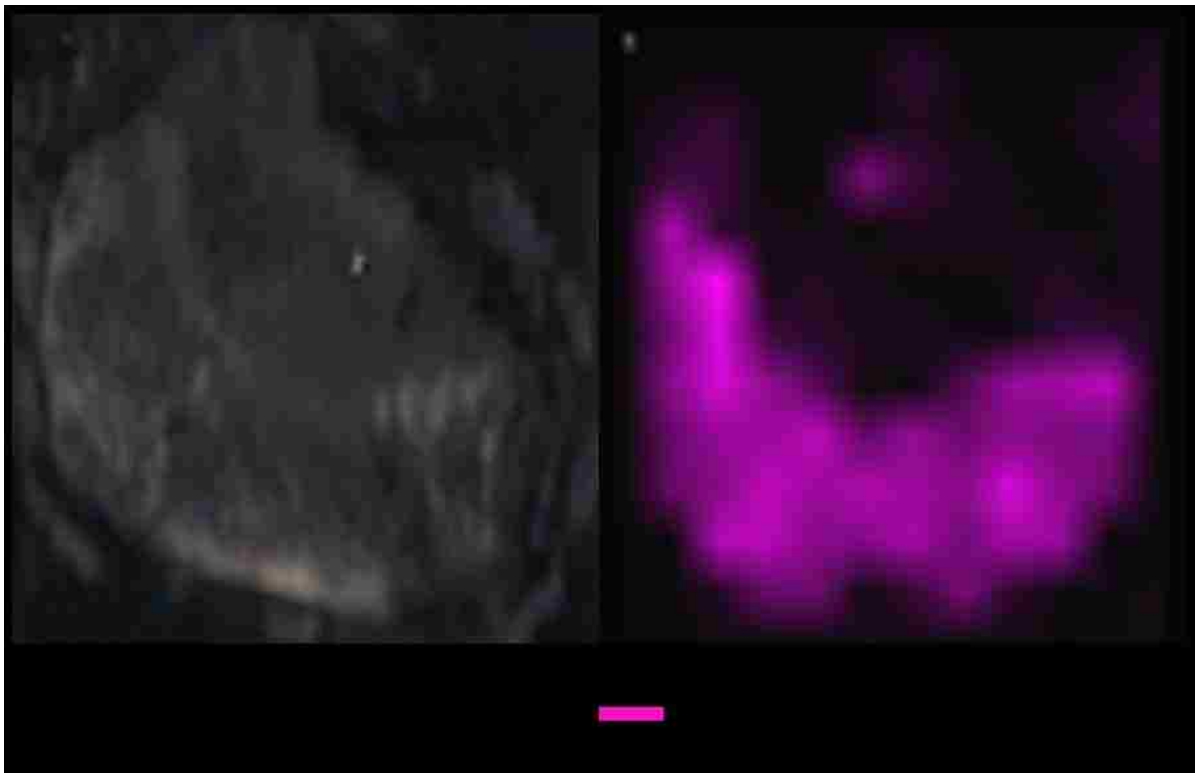

Figure 3.1 (A) Digital (L) and MALDI-TOF MS image of unwashed control tissue spiked with predigested [(50 µM DNP-PLG~MWSR-OH + 530 pM active MMP-9), 37^0 C, 24 hours incubation] with a 600 × 600 μm^2 raster

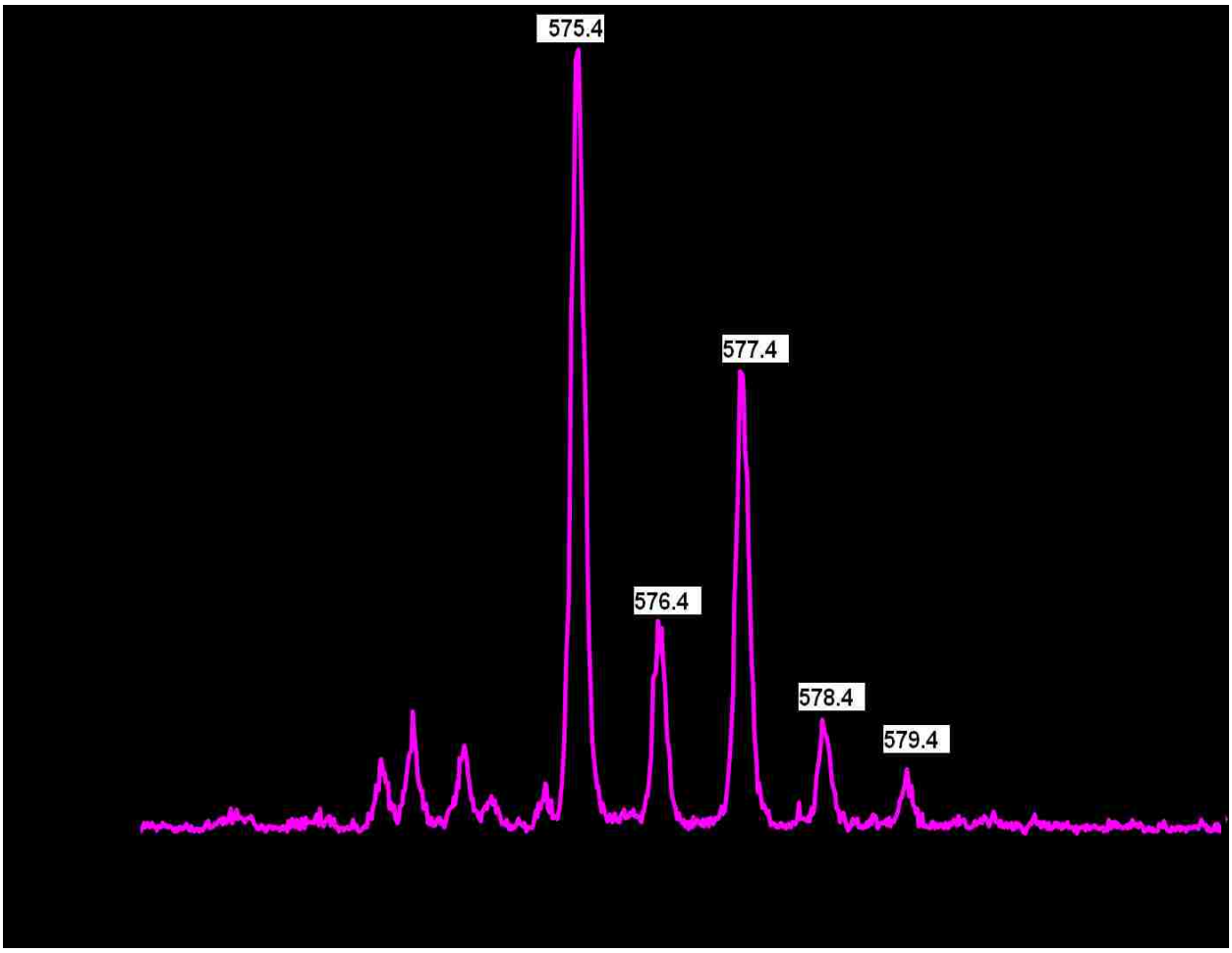

Figure 3.1 (B) MALDI-TOF mass spectrum of unwashed control tissue spiked with predigested [(50 µM DNP-PLG~MWSR-OH + 530 pM active MMP-9), 37^0 C, 24 hours incubation] showing the distribution of lipids from *m/z* 575 – *m/z* 579

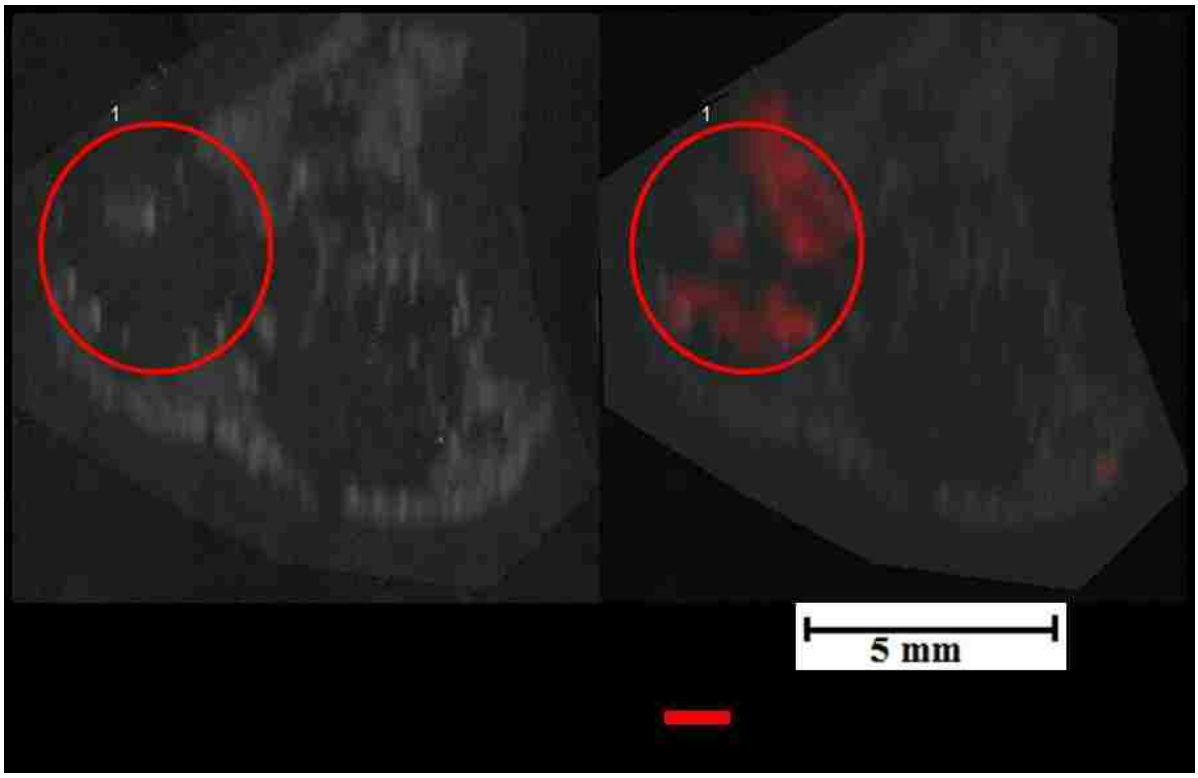

Figure 3.2 Digital (L) and MALDI-TOF MS image of localized MMP-9 activity at a specific region (red circle) on 70/30 v/v% ethanol/water washed control tissue with a 600 × 600 μm^2 raster

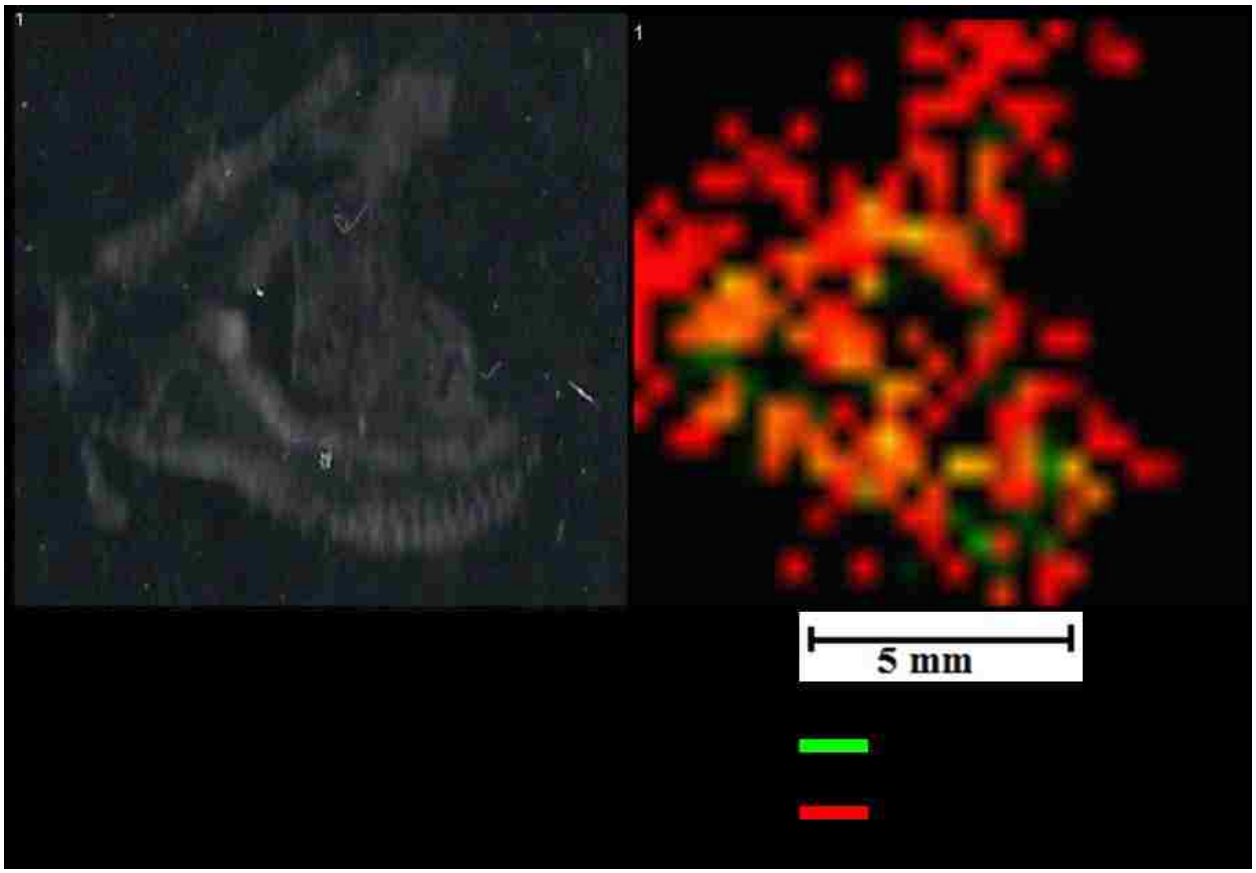

Figure 3.3 Digital (L) and MALDI-TOF MS image (R) of 70/30 v/v% ethanol/water washed control tissue spiked with predigested [(50 µM DNP-PLG~MWSR + 530 pM active MMP-9), 37^0 C, 24 hours incubation] with a 600 × 600 μm^2 raster

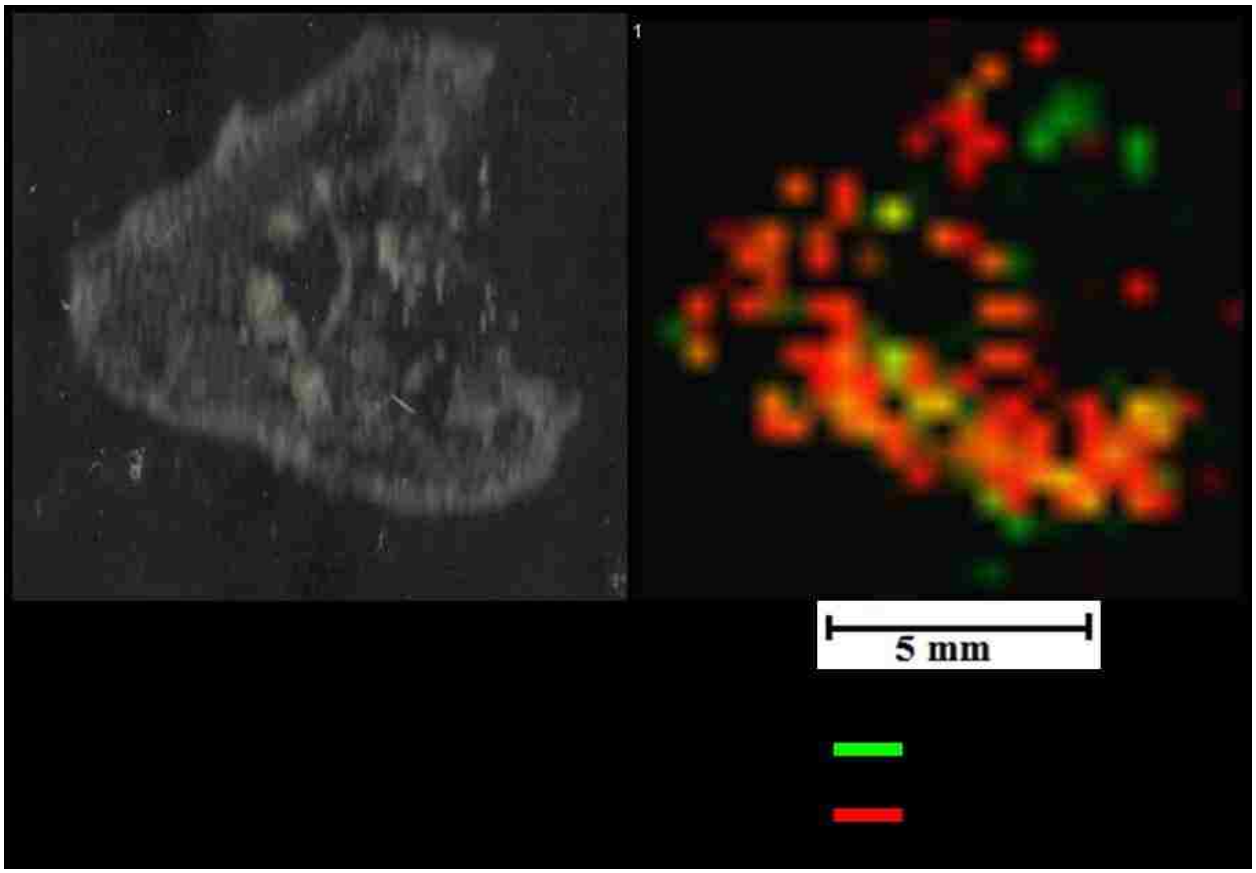

Figure 3.4 Digital (L) and MALDI-TOF MS image (R) of 70/30 v/v% ethanol/water washed control tissue incubated with [50 µM DNP-PLG~MWSR + 530 pM active MMP-9] at 37^0C for 12 hours with a 600 ×600 μm^2 raster

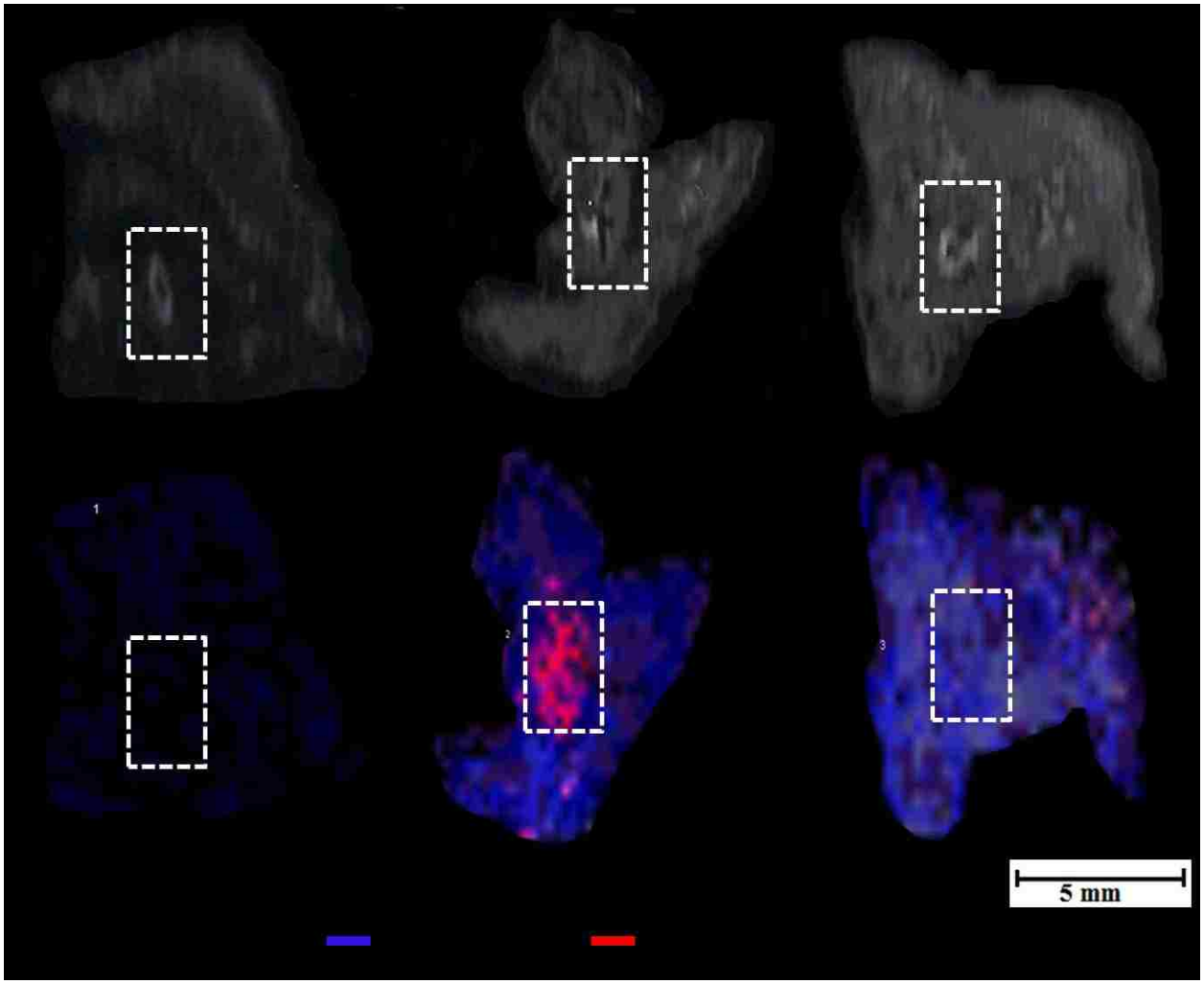

Figure 3.5 Digital (Top) and MALDI-TOF MS (Bottom) image of 70/30 v/v% ethanol/water washed microdialysis probe implanted tissue: (i) without treatment, (ii) incubated with (50 µM DNP-PLG~MWSR + 1X protease inhibitor cocktail), and (iii) incubated with (50 µM DNP-PLG~MWSR + 1X protease inhibitor cocktail + 50 µM GM-6001) [37^0 C, 24 hours incubation] with a 600 × 600 μm^2 raster

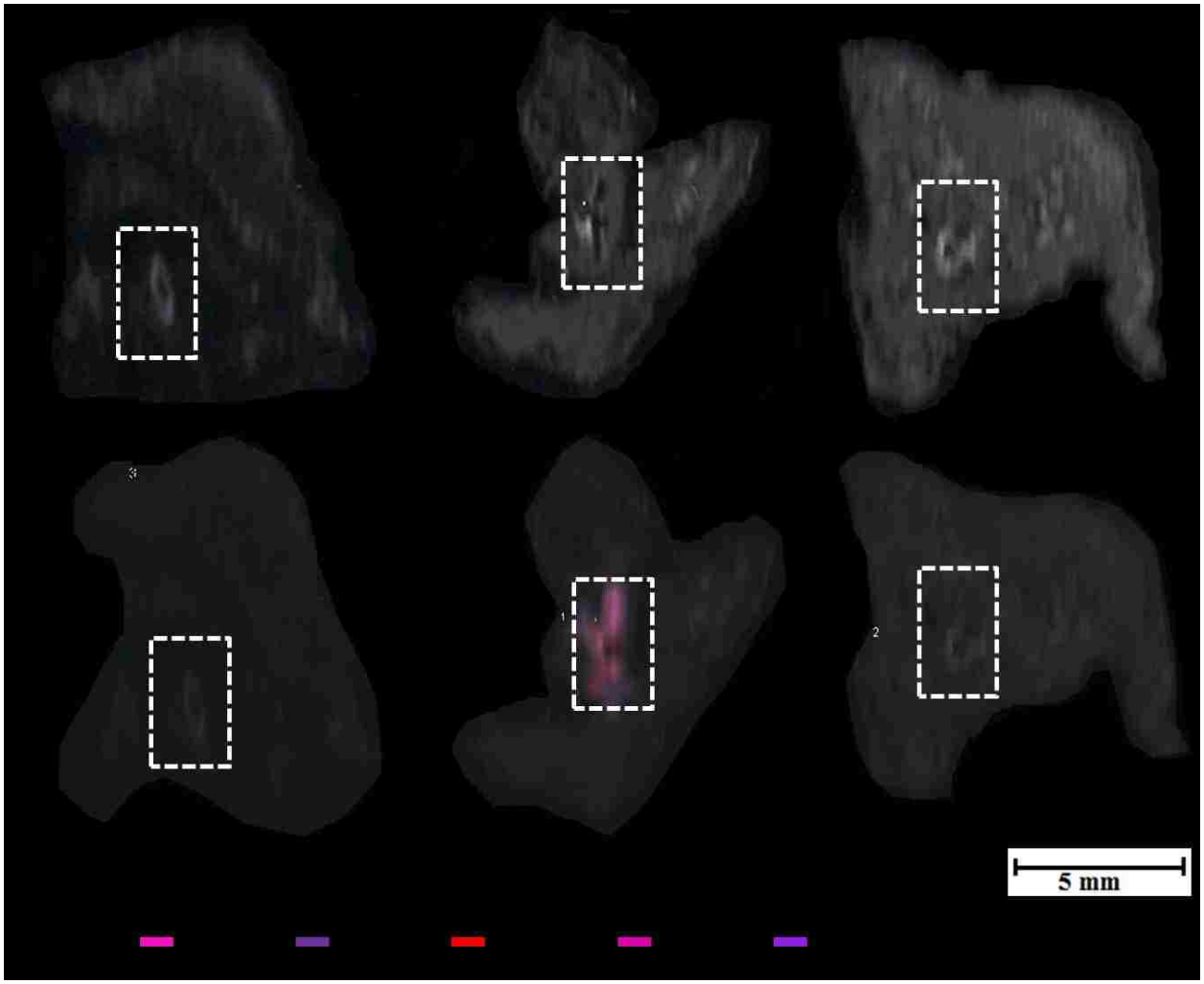

Figure 3.6 (A) Digital (Top) and MALDI-TOF MS/MS (Bottom) image of 70/30 v/v% ethanol/water washed microdialysis probe implanted tissue: (i) without treatment, (ii) incubated with (50 µM DNP-PLG~MWSR + 1X protease inhibitor cocktail), and (iii) incubated with (50 µM DNP-PLG~MWSR + 1X protease inhibitor cocktail + 50 µM GM-6001) [37^0 C, 24 hours incubation] with a 600 × 600 μm^2 raster

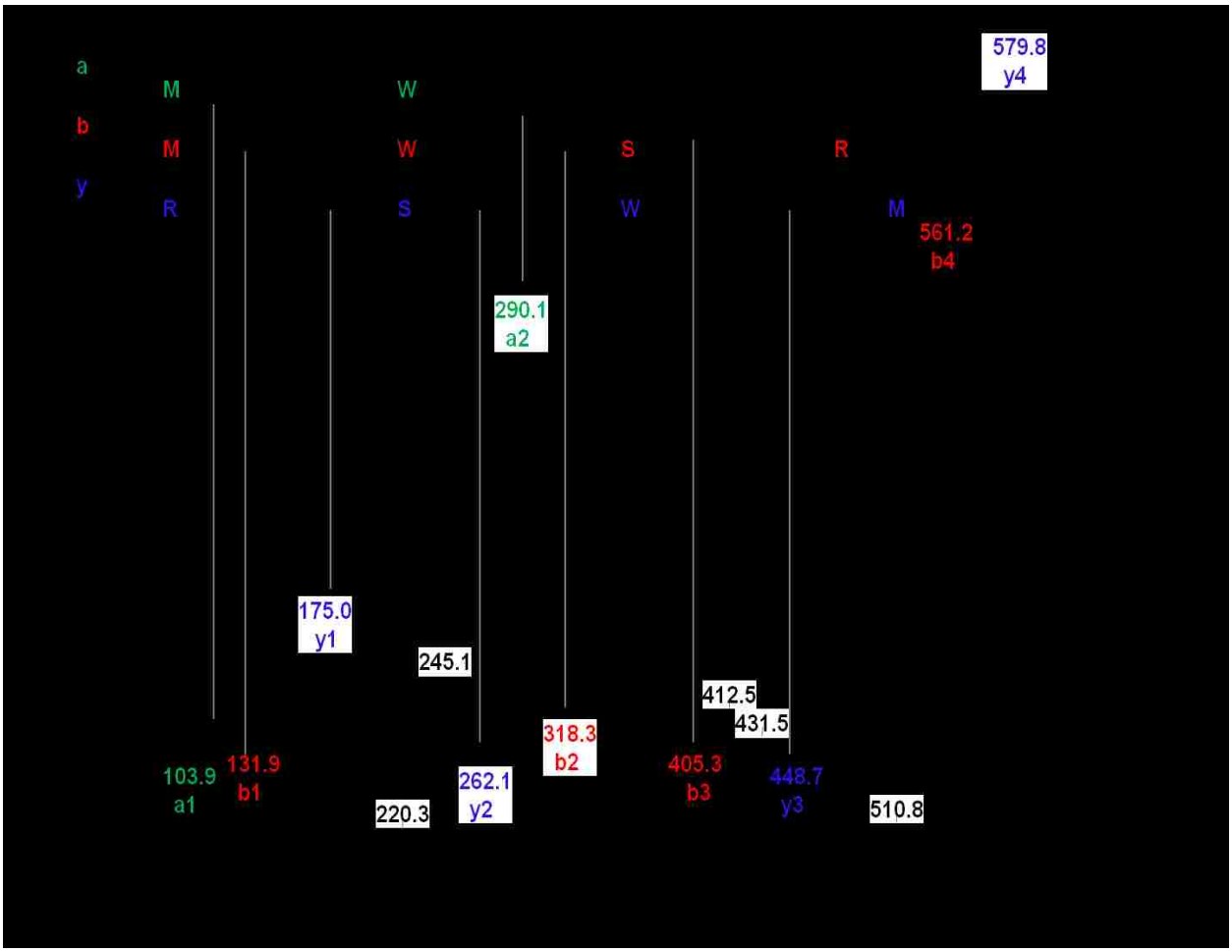

Figure 3.6 (B) MALDI-TOF MS/MS spectrum of the product (*m/z* 579) using the "LIFT" technique

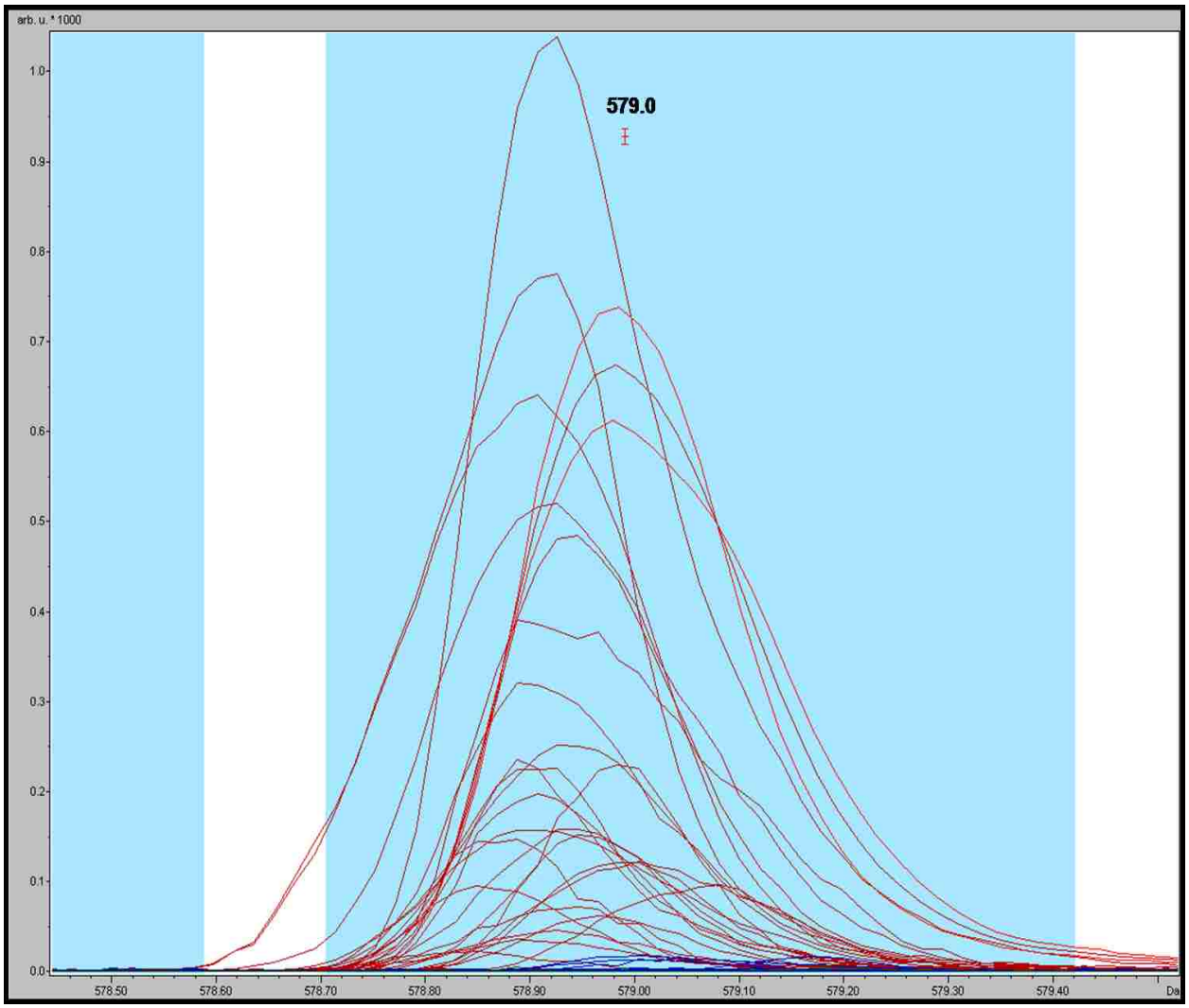

Figure 3.7 (A) Comparison of all single spectral peak intensities of *m/z* 579.0 peak showing significant difference between no treatment (green), treatment (red), and negative treatment (blue) [X-axis: m/z, Y-axis: Intensity (A.U.)]

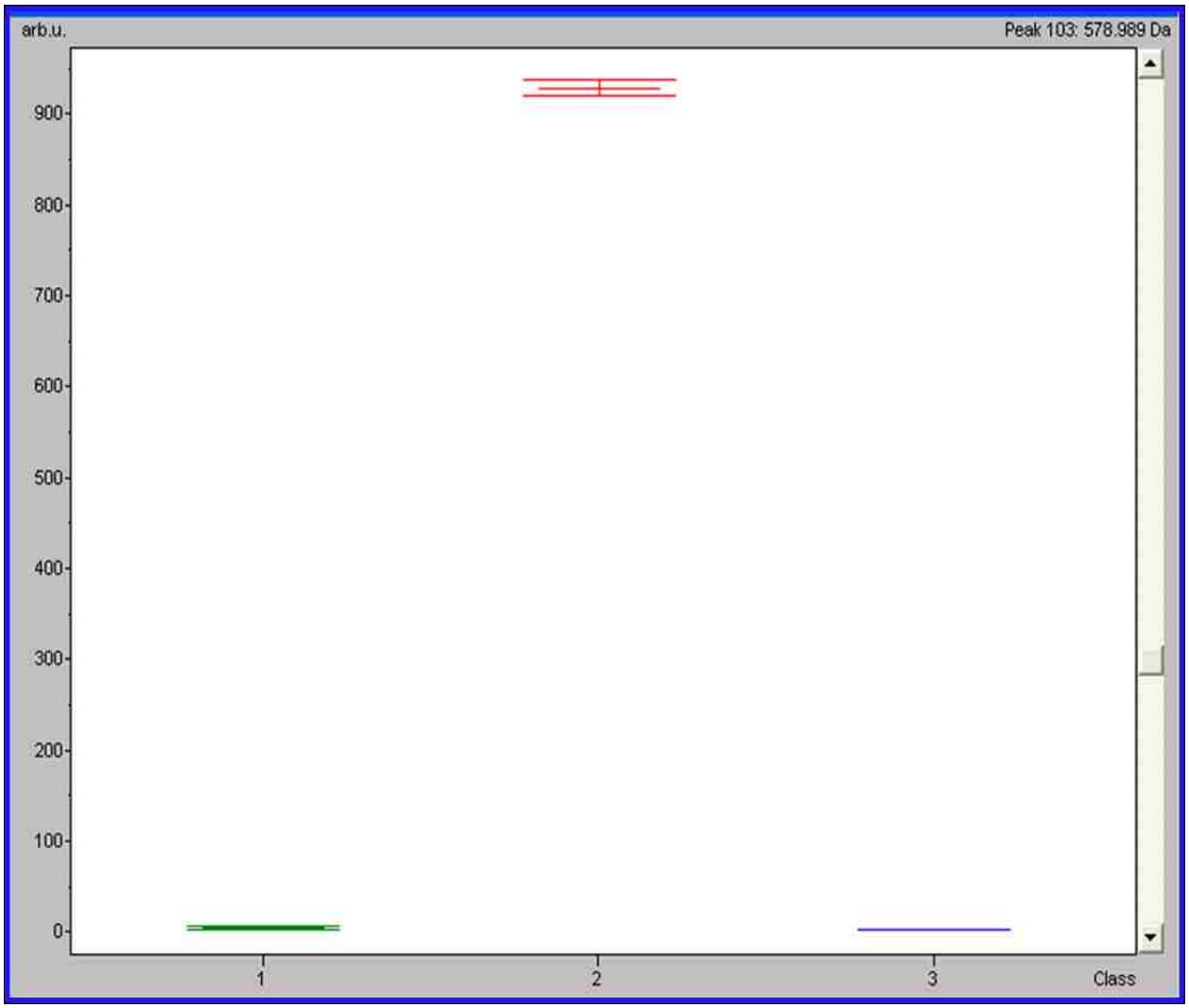

Figure 3.7 (B) Comparison of average spectral intensities of *m/z* 579.0 peak showing significant difference between no treatment (green), treatment (red), and negative treatment (blue) [X-axis: m/z, Y-axis: Intensity (A.U.)]

Mass (*m/z* value)	**579.0**
Difference between the maximal and minimal average peak area of all classes	675.04
P-value of Kruskal-Wallis test	0.0638
P-value of Anderson-Darling test	0.0000357
Peak area intensity of no treatment	3.47
Peak area intensity of treatment	675.9
Peak area intensity of negative control treatment	0.86
Standard deviation of peak area average of no treatment	1.48
Standard deviation of peak area average of treatment	88.93
Standard deviation of peak area average of negative treatment)	0.21
Coefficient of variation in % of no treatment	42.65
Coefficient of variation in % of treatment	13.16
Coefficient of variation in % of negative treatment	24.4

Table 3.1 Peak statistic report using ClinProTools software

B. Fluorescence imaging

The control tissue did not exhibit fluorescence when incubated with the FRET substrate. Alcohol washed microdialysis probe implanted tissues incubated with 10 µM QXL^{TM} 520-Pro-Leu-Gly-Cys(Me)~His-Ala-D-Arg-Lys(5-FAM)-NH_2 exhibited fluorescence around the microdialysis probe indicating the localization of proteolytic activities around the microdialysis probe [Figure 3.8(A)]. Alcohol washed microdialysis probe implanted tissues incubated with (10 µM QXL^{TM} 520-Pro-Leu-Gly-Cys(Me)~His-Ala-D-Arg-Lys(5-FAM)-NH_2 + 50 µM GM-6001) did not block the fluorescence around the microdialysis probe indicating the localization of proteolytic activities not specific for MMPs around the probe [Figure 3.8 (B)].

In order to validate the activity of MMPs, an EDTA-free protease inhibitor cocktail was employed to block the hydrolysis of the substrate by proteases other than MMPs for 70/30 v/v% ethanol/water washed tissue samples [Figure 3.8 (C)]. About 70% of the time, the tissue sample that did not receive any treatment did not show autofluorescence. GM-6001 did not completely block the activity of MMPs.

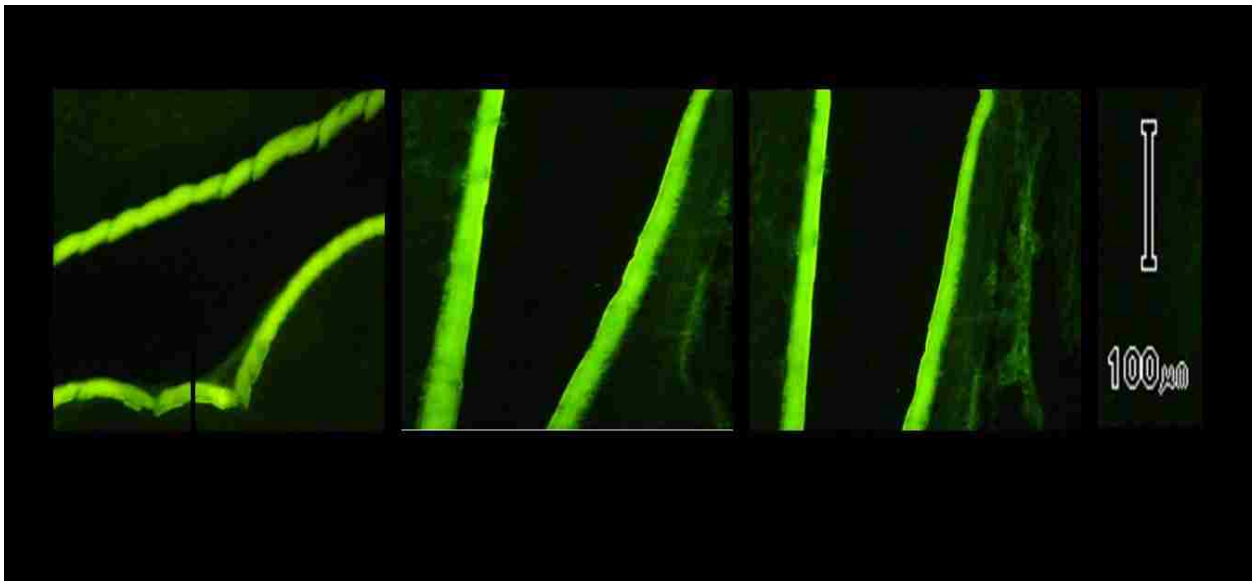

Figure 3.8 (A) Microdialysis probe implanted tissues incubated with 10 µM QXL^{TM} 520-Pro-Leu-Gly-Cys(Me)~His-Ala-D-Arg-Lys(5-FAM)-NH_2 exhibited fluorescence around the microdialysis probe indicating the localization of proteolytic activities around the probe

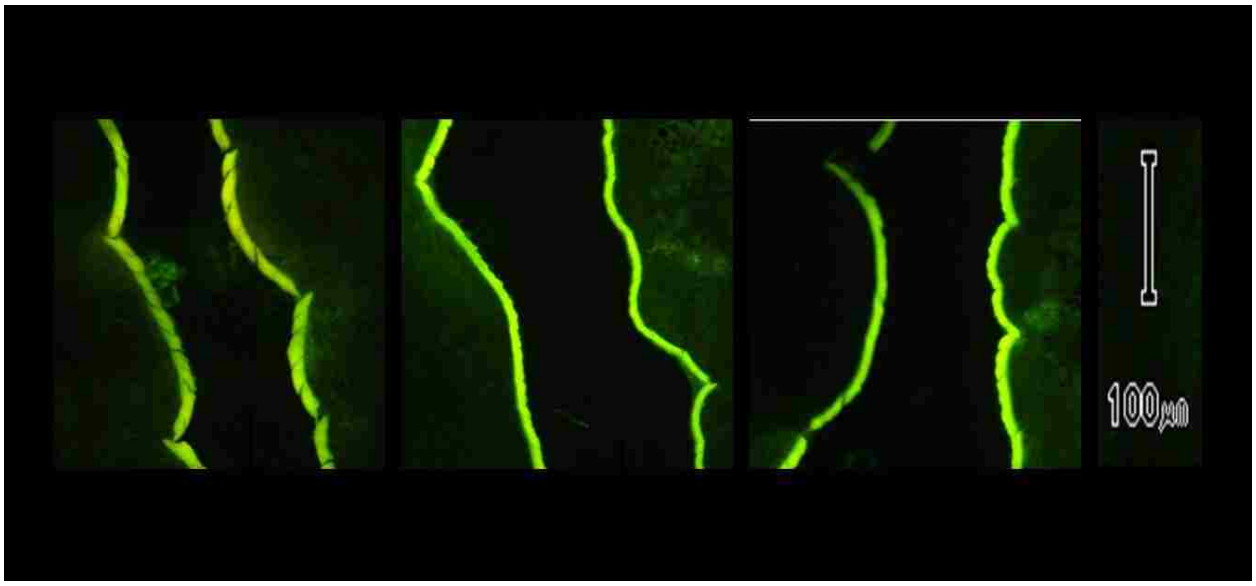

Figure 3.8 (B) Alcohol washed microdialysis probe implanted tissues incubated with (10 µM QXL^{TM} 520-Pro-Leu-Gly-Cys(Me)~His-Ala-D-Arg-Lys(5-FAM)-NH_2 + 50 µM GM-6001) did not block the fluorescence around the probe indicating the localization of proteolytic activities not specific for MMPs around the probe

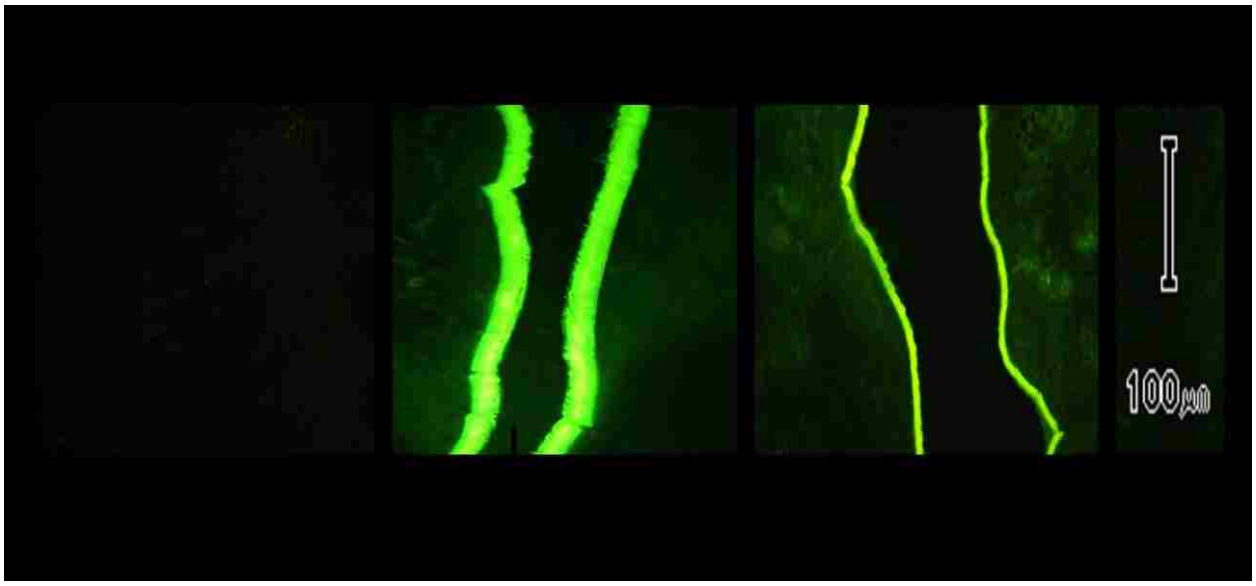

Figure 3.8 (C) 70/30 v/v% ethanol/water washed microdialysis probe implanted tissues: (i) without treatment, (ii) incubated with (10 μM QXL^{TM} 520-Pro-Leu-Gly-Cys(Me)~His-Ala-D-Arg-Lys(5-FAM)-NH_2 + 1X EDTA-free protease inhibitor cocktail), and (iii) incubated with (10 μM QXL^{TM} 520-Pro-Leu-Gly-Cys(Me)~His-Ala-D-Arg-Lys(5-FAM)-NH_2 + 1X EDTA-free protease inhibitor cocktail + 50 μM GM-6001)

3.4 Conclusions

It was not possible to image the localized activity of MMP-2 and MMP-9 in unwashed tissue samples because of signal suppression by lipids. Fluorescence imaging studies indicated that alcohol washing did not completely remove the activity of MMPs. The use of ethanol as washing solvent for MALDI-IMS experiments did not completely remove the lipids. However, the signal suppression effects from interfering lipids were eliminated from the tissue sections to allow the imaging of MMPs activity.

4. SUMMARY AND FUTURE DIRECTIONS

Most of the standard methods to study the localization of active enzymes in tissue samples rely on microscopy and staining/labeling techniques.[75] Visualizing the spatial localization of enzymatic activity using imaging mass spectrometry (IMS) by monitoring the mass difference between the substrate and its product(s) is a novel technique that does not require labeling agents.

However, the use of a labeled substrate might permit simultaneous fluorescence and mass spectrometry imaging on a tissue sample. The longer wavelength FRET substrate ($\lambda_{Ex}/\lambda_{Em}$ = 490 nm/520 nm), QXL™ 520-Pro-Leu-Gly-Cys(Me)~His-Ala-D-Arg-Lys(5-FAM)-NH_2, used in this research was selected solely for this purpose to image the localization of active MMPs in the FBR-induced tissue samples.

QXL™ 520-Pro-Leu-Gly-Cys(Me)~His-Ala-D-Arg-Lys(5-FAM)-NH_2 was found to be an excellent candidate for fluorescence imaging. But, the MMP-9 activity assay performed with this substrate did not prove to be MS-compatible.

On the other hand, the MMP-9 activity assay performed with a shorter wavelength FRET substrate ($\lambda_{Ex}/\lambda_{Em}$ = 280 nm/360 nm), DNP-Pro-Leu-Gly~Met-Trp-Ser-Arg, was compatible with MS. This substrate could not be used for fluorescence imaging studies because of the strong interference from tissue autofluorescence. Hence two different FRET substrates, DNP-Pro-Leu-Gly~Met-Trp-Ser-Arg and QXL™ 520-Pro-Leu-Gly-Cys(Me)~His-Ala-D-Arg-Lys(5-FAM)-NH_2, were used in this research for IMS and fluorescence imaging respectively.

The control tissue sample spiked with predigested (active MMP-9 + DNP-Pro-Leu-Gly~Met-Trp-Ser-Arg) showed ion suppression from lipids indicating the need for an appropriate tissue washing procedure. Alcohols are well known for their delipidation efficiency. Gawlak et al. reported that a combined ethanol and methanol fixation of rat brain tissues at 4^0 C for 6 hours did not negatively affect the activity of MMP-2 and MMP-9.[70] A longer alcohol washing time of 12 hours was selected for this research to achieve efficient removal of lipids. Fluorescence imaging studies with alcohol washed tissue samples were performed to make sure that alcohol washing did not have a negative effect on enzymatic activity. The use of GM-6001 as a negative control in fluorescence imaging studies showed the presence of proteolytic activities not specific for MMPs around the implanted microdialysis probe. Hence, an EDTA-free protease inhibitor cocktail was used to block the activity of proteinases other than MMPs.

Ex vivo tissue studies with DNP-Pro-Leu-Gly~Met-Trp-Ser-Arg and EDTA-free protease inhibitor cocktail revealed the possibility of visualizing the spatial localization of active MMP-2 and MMP-9 in the microdialysis probe implanted tissue by monitoring the product formed at *m/z* 579 using MALDI-TOF imaging MS. The imaging data was validated by using GM-6001, a broad spectrum MMPs inhibitor.

The pixel size of an image is referred to as spatial resolution in IMS.[47] The diameter of the laser beam is the limiting factor in achieving high spatial resolution in MALDI IMS. There is a trade-off between signal intensity and spatial resolution. MALDI IMS data are mostly reported with a pixel size of 50-500 µm. The spatial resolution used for data acquisition in MALDI IMS experiments determines the detail level of the images.[76] In this research, the MALDI MS image was obtained at a spatial resolution of 600 µm without compromising the signal intensity.

Reduced data file size and data acquisition time were the advantages of low spatial resolution. The localization of active MMP-2 and MMP-9 in the microdialysis probe implanted area was clearly visible in the MALDI MS image.

Fluorescence imaging gives a qualitative picture of MMPs activity. MALDI IMS can be made quantitative by considering the fact that the IMS signal is a direct measure of the relative abundance of the analyte.[77] Quantitative information can be obtained by comparing the MALDI MS image of MMPs localization with that of control tissue spiked with known concentrations of the product (*m/z* 579). However, the challenge would be to achieve a homogeneous deposition of the product on the tissue surface that matches with the deposition of the substrate.

The bioanalytical method developed in this research enabled the visualization of localized gelatinases (MMP-2 and MMP-9) activity at the implant site in *ex vivo* tissue samples. In the future, this approach can be extended to visualize the localization of several active MMPs at the implant site in *ex vivo* tissue samples. FRET substrates were used in this research only for the purpose of using fluorescence imaging as a complementary technique. However, a multiplexed assay to visualize the localization of several active MMPs is difficult to achieve in fluorescence imaging because of the limited number of fluorophores that can provide non-overlapping emission bands for the products of MMPs activity. On the other hand, several non-FRET synthetic substrates specific for MMPs of interest can be employed for imaging the localized MMPs activity during the foreign body response in *ex vivo* tissue samples.

References:

1. Helmus, M. N.; Gibbons, D. F.; Cebon, D., Biocompatibility: Meeting a Key Functional Requirement of Next- Generation Medical Devices. *Toxicologic Pathology* **2008,** *36* (1), 70-80.

2. Onuki, Y.; Bhardwaj, U.; Papadimitrakopoulos, F.; Burgess, D. J., A review of the biocompatibility of implantable devices: current challenges to overcome foreign body response. *J Diabetes Sci Technol* **2008,** *2* (6), 1003-15.

3. Luttikhuizen, D. T.; Harmsen, M. C.; Van Luyn, M. J. A., Cellular and molecular dynamics in the foreign body reaction. *Tissue Engineering* **2006,** *12* (7), 1955-1970.

4. Anderson, J. M.; Rodriguez, A.; Chang, D. T., Foreign body reaction to biomaterials. *Seminars in Immunology* **2008,** *20* (2), 86-100.

5. MacLauchlan, S.; Skokos, E. A.; Meznarich, N.; Zhu, D. H.; Raoof, S.; Shipley, J. M.; Senior, R. M.; Bornstein, P.; Kyriakides, T. R., Macrophage fusion, giant cell formation, and the foreign body response require matrix metalloproteinase 9. *Journal of Leukocyte Biology* **2009,** *85* (4), 617-626.

6. Kenneth Ward, W., A review of the foreign-body response to subcutaneously-implanted devices: the role of macrophages and cytokines in biofouling and fibrosis. *J Diabetes Sci Technol* **2008,** *2* (5), 768-77.

7. Saghatelian, A.; Jessani, N.; Joseph, A.; Humphrey, M.; Cravatt, B. F., Activity-based probes for the proteomic profiling of metalloproteases. *Proceedings of the National Academy of Sciences of the United States of America* **2004,** *101* (27), 10000-10005.

8. Moali, C.; Hulmes, D. J. S., Extracellular and cell surface proteases in wound healing: new players are still emerging. *European Journal of Dermatology* **2009,** *19* (6), 552-564.

9. Van Lint, P.; Libert, C., Chemokine and cytokine processing by matrix metalloproteinases and its effect on leukocyte migration and inflammation. *Journal of Leukocyte Biology* **2007,** *82* (6), 1375-1381.

10. Sternlicht, M. D.; Werb, Z., How matrix metalloproteinases regulate cell behavior. *Annual Review of Cell and Developmental Biology* **2001,** *17*, 463-516.

11. Fanjul-Fernandez, M.; Folgueras, A. R.; Cabrera, S.; Lopez-Otin, C., Matrix metalloproteinases: Evolution, gene regulation and functional analysis in mouse models. *Biochimica Et Biophysica Acta-Molecular Cell Research* **2010,** *1803* (1), 3-19.

12. Le, N. T. V.; Xue, M. L.; Castelnoble, L. A.; Jackson, C. J., The dual personalities of matrix metalloproteinases in inflammation. *Frontiers in Bioscience* **2007,** *12*, 1475-1487.

13. Jones, J. A.; McNally, A. K.; Chang, D. T.; Qin, L. A.; Meyerson, H.; Colton, E.; Kwon, I. L. K.; Matsuda, T.; Anderson, J. M., Matrix metalloproteinases and their inhibitors in the foreign body reaction on biomaterials. *Journal of Biomedical Materials Research Part A* **2008,** *84A* (1), 158-166.

14. Manicone, A. M.; McGuire, J. K., Matrix metalloproteinases as modulators of inflammation. *Seminars in Cell & Developmental Biology* **2008,** *19* (1), 34-41.

15. Luttikhuizen, D. T.; van Amerongen, M. J.; de Feijter, P. C.; Petersen, A. H.; Harmsen, M. C.; van Luyn, M. J. A., The correlation between difference in foreign body reaction between implant locations and cytokine and MMP expression. *Biomaterials* **2006,** *27* (34), 5763-5770.

16. Parks, W. C.; Wilson, C. L.; Lopez-Boado, Y. S., Matrix metalloproteinases as modulators of inflammation and innate immunity. *Nature Reviews Immunology* **2004,** *4* (8), 617-629.

17. McQuibban, G. A.; Gong, J. H.; Wong, J. R.; Wallace, J. L.; Clark-Lewis, I.; Overall, C. M., Matrix metalloproteinase processing of monocyte chemoattractant proteins generates CC chemokine receptor antagonists with anti-inflammatory properties in vivo. *Blood* **2002,** *100* (4), 1160-1167.

18. Fingleton, B.; Lynch, C. C., A New Dress Code for MMPs: Cleavage Optional. *Developmental Cell* **2010,** *18* (1), 3-4.

19. Reuben, P. M.; Cheung, H. S., Regulation of matrix metalloproteinase (MMP) gene expression by protein kinases. *Frontiers in Bioscience* **2006,** *11*, 1199-1215.

20. Johnson, L. L.; Dyer, R.; Hupe, D. J., Matrix metalloproteinases. *Current Opinion in Chemical Biology* **1998,** *2* (4), 466-471.

21. Gomis-Ruth, F. X., Catalytic Domain Architecture of Metzincin Metalloproteases. *Journal of Biological Chemistry* **2009,** *284* (23), 15353-15357.

22. Gross, J.; Lapiere, C. M., Collagenolytic activity in amphibian tissues- a tissue culture assay. *Proceedings of the National Academy of Sciences of the United States of America* **1962,** *48* (6), 1014-&.

23. Puente, X. S.; Sanchez, L. M.; Overall, C. M.; Lopez-Otin, C., Human and mouse proteases: A comparative genomic approach. *Nature Reviews Genetics* **2003,** *4* (7), 544-558.

24. Bertini, I.; Fragai, M.; Luchinat, C., Intra- and Interdomain Flexibility in Matrix Metalloproteinases: Functional Aspects and Drug Design. *Current Pharmaceutical Design* **2009,** *15* (31), 3592-3605.

25. Ravanti, L.; Kahari, V. M., Matrix metalloproteinases in wound repair (Review). *International Journal of Molecular Medicine* **2000,** *6* (4), 391-407.

26. Visse, R.; Nagase, H., Matrix metalloproteinases and tissue inhibitors of metalloproteinases - Structure, function, and biochemistry. *Circulation Research* **2003,** *92* (8), 827-839.

27. Page-McCaw, A.; Ewald, A. J.; Werb, Z., Matrix metalloproteinases and the regulation of tissue remodelling. *Nature Reviews Molecular Cell Biology* **2007,** *8* (3), 221-233.

28. Park, H. I.; Ni, J.; Gerkema, F. E.; Liu, D.; Belozerov, V. E.; Sang, Q. X. A., Identification and characterization of human endometase (matrix metalloproteinase-26) from endometrial tumor. *Journal of Biological Chemistry* **2000,** *275* (27), 20540-20544.

29. Van Wart, H. E.; Birkedal-Hansen, H., The cysteine switch a principle of regulation of metalloproteinase activity with potential applicability to the entire matrix metalloproteinase gene family. *Proceedings of the National Academy of Sciences of the United States of America* **1990,** *87* (14), 5578-5582.

30. Pei, D. Q.; Kang, T. B.; Qi, H. X., Cysteine array matrix metalloproteinase (CA-MMP)/MMP-23 is a type II transmembrane matrix metalloproteinase regulated by a single cleavage for both secretion and activation. *Journal of Biological Chemistry* **2000,** *275* (43), 33988-33997.

31. Nagase, H.; Visse, R.; Murphy, G., Structure and function of matrix metalloproteinases and TIMPs. *Cardiovascular Research* **2006,** *69* (3), 562-573.

32. Bode, W.; Fernandez-Catalan, C.; Tschesche, H.; Grams, F.; Nagase, H.; Maskos, K., Structural properties of matrix metalloproteinases. *Cellular and Molecular Life Sciences* **1999,** *55* (4), 639-652.

33. Nagase, H.; Woessner, J. F., Matrix metalloproteinases. *Journal of Biological Chemistry* **1999,** *274* (31), 21491-21494.

34. Overall, C. M., Molecular determinants of metalloproteinase substrate specificity - Matrix metalloproteinase substrate binding domains, modules, and exosites. *Molecular Biotechnology* **2002,** *22* (1), 51-86.

35. Sardy, M., Role of Matrix Metalloproteinases in Skin Ageing. *Connective Tissue Research* **2009,** *50* (2), 132-138.

36. Somerville, R. P. T.; Oblander, S. A.; Apte, S. S., Matrix metalloproteinases: old dogs with new tricks. *Genome Biology* **2003,** *4* (6), 11.

37. Stamenkovic, I., Extracellular matrix remodelling: the role of matrix metalloproteinases. *Journal of Pathology* **2003,** *200* (4), 448-464.

38. Cawston, T. E.; Mercer, E., Preferential binding of collagenase to alpha-2-macroglobulin in the presence of the tissue inhibitor of metalloproteinases. *Febs Letters* **1986,** *209* (1), 9-12.

39. Oh, J.; Takahashi, R.; Kondo, S.; Mizoguchi, A.; Adachi, E.; Sasahara, R. M.; Nishimura, S.; Imamura, Y.; Kitayama, H.; Alexander, D. B.; Ide, C.; Horan, T. P.; Arakawa, T.; Yoshida, H.; Nishikawa, S. I.; Itoh, Y.; Seiki, M.; Itohara, S.; Takahashi, C.; Noda, M., The membrane-anchored MMP inhibitor RECK is a key regulator of extracellular matrix integrity and angiogenesis. *Cell* **2001,** *107* (6), 789-800.

40. Catterall, J. B.; Cawston, T. E., Assays of Matrix Metalloproteinases (MMPs) and MMP Inhibitors: Bioassays and Immunoassays Applicable to Cell Culture Medium, Serum, and Synovial Fluid. *METHODS IN MOLECULAR BIOLOGY -CLIFTON THEN TOTOWA-* **2003,** *225*, 353-364.

41. Clark, I. M., *Matrix metalloproteinase protocols*. Humana Press: Totowa, NJ, 2001; Clark, I. M., *Matrix metalloproteinase protocols*. Humana Press: Totowa, N.J., 2001.

42. Mungall, B. A.; Pollitt, C. C., In situ zymography: topographical considerations. *Journal of Biochemical and Biophysical Methods* **2001,** *47* (3), 169-176.

43. Cheng, X. C.; Fang, H.; Xu, W. F., Advances in assays of matrix metalloproteinases (MMPs) and their inhibitors. *Journal of Enzyme Inhibition and Medicinal Chemistry* **2008,** *23* (2), 154-167.

44. Baruch, A.; Jeffery, D. A.; Bogyo, M., Enzyme activity - it's all about image. *Trends in Cell Biology* **2004,** *14* (1), 29-35.

45. Weissleder, R.; Tung, C. H.; Mahmood, U.; Bogdanov, A., In vivo imaging of tumors with protease-activated near-infrared fluorescent probes. *Nature Biotechnology* **1999,** *17* (4), 375-378.

46. Heeren, R. M. A.; Smith, D. F.; Stauber, J.; Kukrer-Kaletas, B.; MacAleese, L., Imaging Mass Spectrometry: Hype or Hope? *Journal of the American Society for Mass Spectrometry* **2009,** *20* (6), 1006-1014.

47. McDonnell, L. A.; Heeren, R. M. A., Imaging mass spectrometry. *Mass Spectrometry Reviews* **2007,** *26* (4), 606-643.

48. Altelaar, A. F. M.; Luxembourg, S. L.; McDonnell, L. A.; Piersma, S. R.; Heeren, R. M. A., Imaging mass spectrometry at cellular length scales. *Nature Protocols* **2007,** *2* (5), 1185-1196.

49. Chaurand, P.; Schwartz, S. A.; Caprioli, R. M., Assessing protein patterns in disease using imaging mass spectrometry. *Journal of Proteome Research* **2004,** *3* (2), 245-252.

50. Glish, G. L.; Vachet, R. W., The basics of mass spectrometry in the twenty-first century. *Nature Reviews Drug Discovery* **2003,** *2* (2), 140-150.

51. Watson, J. T.; Sparkman, O. D., *Introduction to mass spectrometry : instrumentation, applications and strategies for data interpretation*. John Wiley & Sons: Chichester, England; Hoboken, NJ, 2007.

52. Suckau, D.; Resemann, A.; Schuerenberg, M.; Hufnagel, P.; Franzen, J.; Holle, A., A novel MALDI LIFT-TOF/TOF mass spectrometer for proteomics. *Analytical and Bioanalytical Chemistry* **2003,** *376* (7), 952-965.

53. Hardesty, W. M.; Caprioli, R. M., In situ molecular imaging of proteins in tissues using mass spectrometry. *Analytical and Bioanalytical Chemistry* **2008,** *391* (3), 899-903.

54. Kruse, R.; Sweedler, J. V., Spatial profiling invertebrate ganglia using MALDI MS. *Journal of the American Society for Mass Spectrometry* **2003,** *14* (7), 752-759.

55. Seeley, E. H.; Oppenheimer, S. R.; Mi, D.; Chaurand, P.; Caprioli, R. M. In *Enhancement of protein sensitivity for MALDI imaging mass spectrometry after chemical treatment of tissue sections*, Elsevier Science Inc: 2008; pp 1069-1077.

56. Schwartz, S. A.; Reyzer, M. L.; Caprioli, R. M., Direct tissue analysis using matrix-assisted laser desorption/ionization mass spectrometry: practical aspects of sample preparation. *Journal of Mass Spectrometry* **2003,** *38* (7), 699-708.

57. Eijkel, G. B.; Kaletas, B. K.; van der Wiel, I. M.; Kros, J. M.; Luider, T. M.; Heeren, R. M. A., Correlating MALDI and SIMS imaging mass spectrometric datasets of biological tissue surfaces. *Surface and Interface Analysis* **2009,** *41* (8), 675-685.

58. Greis, K. D., Mass spectrometry for enzyme assays and inhibitor screening: An emerging application in pharmaceutical research. *Mass Spectrometry Reviews* **2007,** *26* (3), 324-339.

59. Mandal, M.; Mandal, A.; Das, S.; Chakraborti, T.; Chakraborti, S., Clinical implications of matrix metalloproteinases. *Molecular and Cellular Biochemistry* **2003,** *252* (1-2), 305-329.

60. Witte, M. B.; Thornton, F. J.; Kiyama, T.; Efron, D. T.; Schulz, G. S.; Moldawer, L. L.; Barbul, A. In *Metalloproteinase inhibitors and wound healing: A novel enhancer of wound strength*, Mosby-Year Book Inc: 1998; pp 464-470.

61. Leib, S. L.; Leppert, D.; Clements, J.; Tauber, M. G., Matrix metalloproteinases contribute to brain damage in experimental pneumococcal meningitis. *Infection and Immunity* **2000,** *68* (2), 615-620.

62. Stepicheva; nbsp; N. Altered lipid composition of melanosomal membranes in Smyth line chickens with autoimmune vitiligo. M.S., University of Arkansas, United States -- Arkansas, 2011.

63. Schwamborn, K.; Krieg, R. C.; Reska, M.; Jakse, G.; Knuechel, R.; Wellmann, A., Identifying prostate carcinoma by MALDI-Imaging. *International Journal of Molecular Medicine* **2007,** *20* (2), 155-159.

64. Zaima, N.; Hayasaka, T.; Goto-Inoue, N.; Setou, M., Imaging of Metabolites by MALDI Mass Spectrometry. *Journal of Oleo Science* **2009,** *58* (8), 415-419.

65. Okada, Y.; Gonoji, Y.; Naka, K.; Tomita, K.; Nakanishi, I.; Iwata, K.; Yamashita, K.; Hayakawa, T., Matrix metalloproteinase -9(92-KDa gelatinase type-IV collagenase) from HT-1080 human fibrosarcoma cells - Purification and activation of the precursor and enzymatic-properties. *Journal of Biological Chemistry* **1992,** *267* (30), 21712-21719.

66. Snoek-van Beurden, P. A. M.; Von den Hoff, J. W., Zymographic techniques for the analysis of matrix metalloproteinases and their inhibitors. *Biotechniques* **2005,** *38* (1), 73-83.

67. Jambovane, S.; Kim, D. J.; Duin, E. C.; Kim, S.-K.; Hong, J. W., Creation of Stepwise Concentration Gradient in Picoliter Droplets for Parallel Reactions of Matrix Metalloproteinase II and IX. *Analytical Chemistry* **2011**, null-null.

68. Fiore, E.; Fusco, C.; Romero, P.; Stamenkovic, I., Matrix metalloproteinase 9 (MMP-9/gelatinase B) proteolytically cleaves ICAM-1 and participates in tumor cell resistance to natural killer cell-mediated cytotoxicity. *Oncogene* **2002,** *21* (34), 5213-5223.

69. von Grote, E. C.; Venkatakrishnan, V.; Duo, J.; Stenken, J. A., Long-term subcutaneous microdialysis sampling and qRT-PCR of MCP-1, IL-6 and IL-10 in freely-moving rats. *Molecular Biosystems* **2011,** *7* (1), 150-161.

70. Gawlak, M.; Gorkiewicz, T.; Gorlewicz, A.; Konopacki, F. A.; Kaczmarek, L.; Wilczynski, G. M., High resolution in situ zymography reveals matrix metalloproteinase activity at glutamatergic synapses. *Neuroscience* **2009,** *158* (1), 167-176.

71. Altelaar, A. F. M.; Taban, I. M.; McDonnell, L. A.; Verhaert, P.; de Lange, R. P. J.; Adan, R. A. H.; Mooi, W. J.; Heeren, R. M. A.; Piersma, S. R., High-resolution MALDI imaging mass spectrometry allows localization of peptide distributions at cellular length scales in pituitary tissue sections. *International Journal of Mass Spectrometry* **2007,** *260* (2-3), 203-211.

72. Grey, A. C.; Chaurand, P.; Caprioli, R. M.; Schey, K. L., MALDI Imaging Mass Spectrometry of Integral Membrane Proteins from Ocular Lens and Retinal Tissue. *Journal of Proteome Research* **2009,** *8* (7), 3278-3283.

73. Beekman, B.; vanEl, B.; Drijfhout, J. W.; Ronday, H. K.; TeKoppele, J. M., Highly increased levels of active stromelysin in rheumatoid synovial fluid determined by a selective fluorogenic assay. *Febs Letters* **1997,** *418* (3), 305-309.

74. Seeley, E. H.; Caprioli, R. M., Molecular imaging of proteins in tissues by mass spectrometry. *Proceedings of the National Academy of Sciences of the United States of America* **2008,** *105* (47), 18126-18131.

75. Svatos, A., Mass spectrometric imaging of small molecules. *Trends in Biotechnology* **2010,** *28* (8), 425-434.

76. Snel, M. F.; Fuller, M., High-Spatial Resolution Matrix-Assisted Laser Desorption Ionization Imaging Analysis of Glucosylceramide in Spleen Sections from a Mouse Model of Gaucher Disease. *Analytical Chemistry* **2010,** *82* (9), 3664-3670.

77. Koeniger, S. L.; Talaty, N.; Luo, Y. P.; Ready, D.; Voorbach, M.; Seifert, T.; Cepa, S.; Fagerland, J. A.; Bouska, J.; Buck, W.; Johnson, R. W.; Spanton, S., A quantitation method for mass spectrometry imaging. *Rapid Communications in Mass Spectrometry* **2011,** *25* (4), 503-510.